AGU PUBLICATIONS

JGR

Journal of Geophysical Research: Solid Earth

RESEARCH ARTICLE
10.1002/2015JB012202

The role of passive margins on the evolution of Subduction-Transform Edge Propagators (STEPs)

Nicolai Nijholt[1] and Rob Govers[1]

[1]Department of Earth Sciences, Utrecht University, Utrecht, Netherlands

Key Points:
- STEPs readily track passive margins in a specific range of geometries
- STEP evolution fairly insensitive to lateral strength contrast at passive margin
- Subduction history does not significantly affect the STEP propagation direction

Supporting Information:
- Figure S1
- Figure S2
- Figure S3
- Figure S4
- Figure S5
- Texts S1–S6

Correspondence to:
N. Nijholt,
n.nijholt@uu.nl

Citation:
Nijholt, N., and R. Govers (2015), The role of passive margins on the evolution of Subduction-Transform Edge Propagators (STEPs), *J. Geophys. Res. Solid Earth*, *120*, 7203–7230, doi:10.1002/2015JB012202.

Received 13 MAY 2015
Accepted 2 SEP 2015
Accepted article online 5 SEP 2015
Published online 5 OCT 2015

Abstract A Subduction-Transform Edge Propagator (STEP) is the locus of continual lithospheric tearing which enables subduction of one part of a tectonic plate, while the juxtaposed part remains at the surface. A key question is the propagation direction of active STEPs, and we suspect passive margins to play a critical role in steering STEPs. We investigate the role of passive margins (width, orientation, and lateral strength contrast) on the STEP propagation direction through mechanical finite element models. For straight passive margins, we show that STEPs remain parallel to passive margins when within 15° from a trench-perpendicular geometry. In other cases, where passive margins change strike ahead of the active STEP, STEPs are captured by passive margins for abrupt strike changes (radius of curvature $<$ lithosphere thickness) less than 25° from trench perpendicular. Outside this window, STEPs will propagate in the original direction. If a strike change ($>$25°) is made through a large radius of curvature ($>$lithosphere thickness), STEPs will also propagate along the passive margin. A STEP system evolves toward orthogonality, which may explain why STEP faults are approximately perpendicular to trenches in nature. STEP systems are relatively insensitive to small-scale details (due to large-scale stresses), propagating as straight features along rugged passive margins. Surprisingly, magnitudes of lithospheric strength variation across the passive margin and subduction history, which determines location and magnitude of density anomalies in the mantle, are less relevant for the STEP propagation direction.

1. Introduction

At the lateral edges of subduction zones, continual lithospheric tearing is a consequence of the geodynamic setting. Vertical tearing of the plate at the surface enables that subduction can continue [*Wilson*, 1965; *Isacks et al*., 1969; *Forsyth*, 1975; *Millen and Hamburger*, 1998]. The locus of active lithospheric tearing is defined as a Subduction-Transform Edge Propagator (STEP) [*Govers and Wortel*, 2005]. In the wake of a propagating STEP, a plate boundary develops between the overriding and subducting plates, defined as the STEP fault [*Baes et al*., 2011]. Tearing at the active STEP depends on both the driving forces (mostly slab pull) and on the forces resisting propagation (plate boundary friction and lithosphere strength [*Govers and Wortel*, 2005]). The kinematics on the STEP fault between the surface segment of the broken plate and the overriding plate are strongly affected by the tectonic setting: e.g., in a Mediterranean-like setting relative motions on a STEP fault vary strongly along strike.

In the southwest Pacific region, the northern termination of the Tonga trench and eastern termination of the New Hebrides trench (Figure 1) represent relatively simple examples of lithospheric tearing and STEP system evolution [*Isacks et al*., 1969; *Millen and Hamburger*, 1998; *Govers and Wortel*, 2005; *Wortel et al*., 2009]. The Vityaz lineament represents a broad deformation zone divided into two segments (Figure 1). The western segment (extending west from Fiji; dashed red line in Figure 1) is the trace of a paleotrench (Vityaz trench in *Hall* [2002], *Hall and Spakman* [2002], *Wortel et al*. [2009], and *Schellart and Spakman* [2012]). The eastern segment (extending east from Fiji; solid red line in Figure 1) is the STEP fault, active since at least 7 Ma [*Wortel et al*., 2009]. The two STEPs at both ends of the Tonga and New Hebrides trenches have propagated approximately perpendicular to the trench as highlighted by the orientation of their related STEP faults and the alignment of the (deep) slab edge (Figure 1).

Govers and Wortel [2005] study 3-D numerical models of STEP systems and use Coulomb stresses to predict fault propagation directions. In the absence of lateral variations in mechanical properties, the STEP will continue to propagate approximately parallel to the previously developed STEP fault. Both the subducting Pacific plate near the Tonga subduction zone and the subducting Australian plate near the New Hebrides subduction zone can be considered approximately uniform. In case no lateral variations in mechanical properties are present, STEP

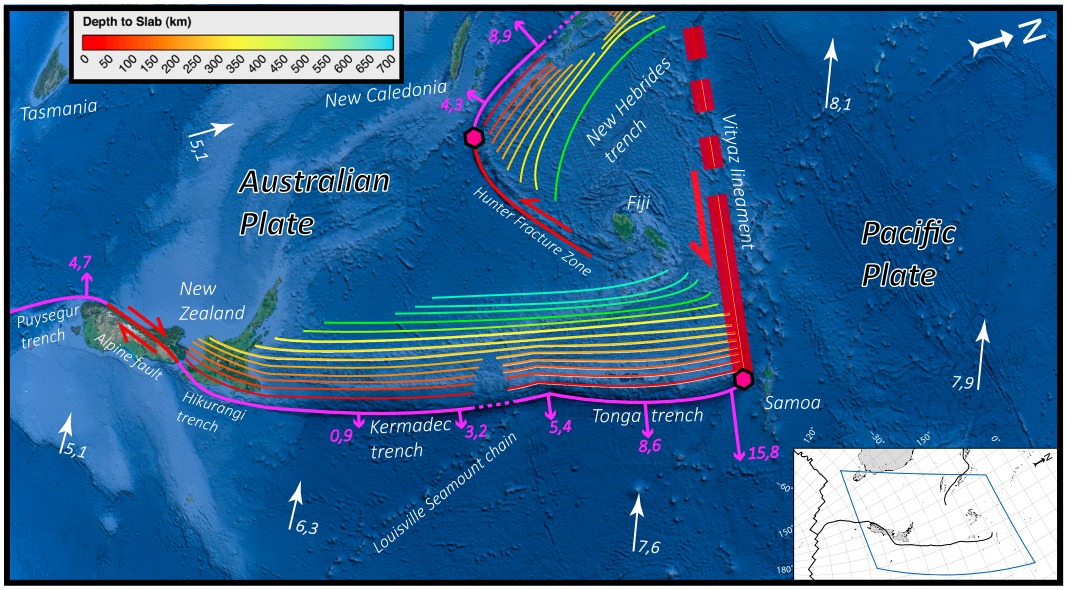

Figure 1. Regional topographic/bathymetric map of the southwest Pacific region, including the isodepth contours of the subducting plates. The white arrows represent plate velocities in the Indo-Atlantic moving hot spot reference frame, while the pink arrows indicate trench-perpendicular retreat velocities (after *Schellart et al.* [2007] and *Schellart and Spakman* [2012]). The magenta hexagons indicate active STEPs. STEP faults at the northern termination of the Tonga trench and eastern termination of the New Hebrides trench are shown as deformation zones, with an overall sinistral sense of shear, modified after the Slab1.0 model [*Hayes et al.*, 2012] and tomography models BS2000 in *Bijwaard and Spakman* [2000] and in *Wortel et al.* [2009] and UU-P07 in *Schellart and Spakman* [2012].

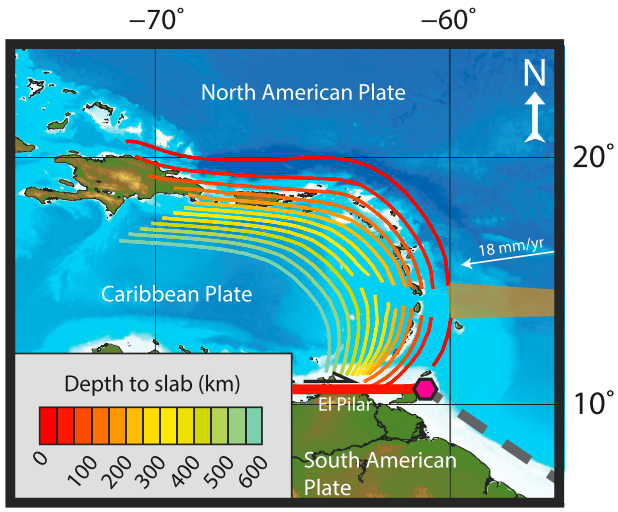

Figure 2. Regional topographic/bathymetric map of the Caribbean region. The red to green lines parallel to the trench are isodepth contours (inset) from the surface down to the subducted slab. This denotes the location of the convergent plate boundary in dark red, i.e., where the slab depth is 0 km. The brown region indicates the diffuse boundary between the North and South American plates (after *van Benthem et al.* [2013]). The grey dashed line indicates the end of the South American passive margin. The STEP fault (El Pilar fault zone) has a dextral sense of shear, modified after *Gudmundsson and Sambridge* [1998] and *Austermann et al.* [2013] and tomography model UU-P07 in *van Benthem et al.* [2013].

fault-parallel (or trench-perpendicular) propagation seems to represent a suitable first-order response for STEP systems [*Govers and Wortel*, 2005].

At the south Lesser Antilles subduction zone, seismic tomographic images of the upper mantle show an edge along the south Lesser Antilles slab, that roughly aligns with the STEP fault (El Pilar fault zone) between the surface plates [*van Benthem et al.*, 2013]. This STEP fault is located along the margin of the continental South American lithosphere (Figure 2 [*Govers and Wortel*, 2005; *van Benthem et al.*, 2013]). We suspect that the coincidence of the STEP fault and the passive margin is a consequence of rupturing along the mechanical strength contrast there. It is important to keep in mind that alignment of a (deep) slab edge and the shallow STEP fault is more indicative of propagation parallel to the passive margin than the local orientation of the trench relative to the margin at the trench-STEP fault intersection, which may be the result of an intricate interplay of friction/resistance to tearing.

Here we focus on the influence of lateral variations in mechanical strength of the lithosphere, due to the presence of a passive margin, on the direction of STEP propagation. Specifically, we are interested in the geometric relationship in time of passive margins, STEP faults, and trenches. Old oceanic lithosphere has large lithospheric strength and as such a large resistance to tearing [*Kohlstedt et al*., 1995]. Continental lithosphere is less strong and has less resistance to tearing [*Kohlstedt et al*., 1995]. Passive margins therefore represent major discontinuities in lithospheric strength. Analog and numerical models in convergent settings, which include two (or possibly more) domains with different material properties, indicate localization of strain along heterogeneities [e.g., *England and Houseman*, 1985; *Dayem et al*., 2009; *Calignano et al*., 2015]. This localization occurs in the weaker material adjacent to the stronger material. As passive margins represent a first-order contrast in rock mechanical properties, one can expect that they may play a critical role in the propagation direction of a STEP.

We use mechanical finite element models which include passive margins in a STEP system and study the effect of the strike of a passive margin with respect to the trench, the magnitude of the lithospheric strength variation across the passive margin, and the subduction history (through the resulting slab pull force). First, we review tectonic settings of natural STEP systems as a basis for our generic models. Next, we investigate uniform models followed by more complex settings including passive margins with various structures. We will subsequently analyze and discuss our results to determine what controls the STEP propagation direction, especially concerning the orientation of the passive margin.

2. Tectonic Setting of STEP Systems

Subduction-Transform Edge Propagators require lithospheric tearing to propagate. The surface geometry found in nature is one where subduction and STEP fault are oriented approximately perpendicular. Examples of such geometry are the northern termination of the Tonga subduction zone, the eastern end of the New Hebrides trench, the southern termination of the south Lesser Antilles trench, both terminations of the South Sandwich trench, both terminations of the Gibraltar arc, the western end of the Sulawesi trench, both terminations of the Calabrian subduction zone, and both terminations of the Hellenic subduction zone [*Millen and Hamburger*, 1998; *Govers and Wortel*, 2005; *Clark et al*., 2008; *Gutscher et al*., 2012; *Özbakir et al*., 2013; *van Benthem et al*., 2013]. At the south Lesser Antilles and Gibraltar arcs, the STEP fault is located along the margin of the continental plate [*Govers and Wortel*, 2005; *Clark et al*., 2008; *Gutscher et al*., 2012].

The perpendicular character of the observed STEP systems in nature is striking, which then raises the question whether the orthogonality of STEP fault and trench is a transient feature or, rather, the preferred setup toward which a STEP system will evolve. Also, the amount of STEPs along a passive margin in nature is limited which does not provide direct evidence on the steering effect of passive margins on STEP propagation. Even though slab rollback and STEP propagation resulted in the development of the (trace of the) El Pilar fault zone since ~45 Ma [*van Benthem et al*., 2013] at the south Lesser Antilles subduction zone, this may simply be a coincidence if the STEP was already perpendicular to the trench when approaching the South American passive margin which fortuitously arrived in its path. The alignment of the deep slab edge in the mantle transition zone with the South American passive margin (Figure 2) and the longevity of the system suggest that it is a very stable setup which is not in a transient phase. Here we seek to determine whether propagation along a margin is a stable geodynamic feature as inferred from the south Lesser Antilles arc evolution. A passive margin may or may not be key in steering this STEP, and we will determine whether the orthogonality of STEP fault and trench is a transient feature or the preferred setup for a STEP system by systematically reviewing setups of STEP systems, including both perpendicular and nonperpendicular STEP settings.

3. Numerical Model Approach for STEP Systems

3.1. General

Keeping the geometry of the south Lesser Antilles subduction zone in mind, we investigate models including a straight passive margin oriented at different angles with respect to a straight trench (Figure 3). In our 2-D, mechanical models, we take an average of the rheological properties of the layered lithosphere to a single parameter: the effective lithospheric viscosity (instead of the integrated strength) of a thin plate. We calculate the transmission of slab pull into the surface plate in a separate set of models (Appendix A) and let the tectonic forces (prescribed velocities and slab pull) act on the appropriate domain interfaces (Figure 3).

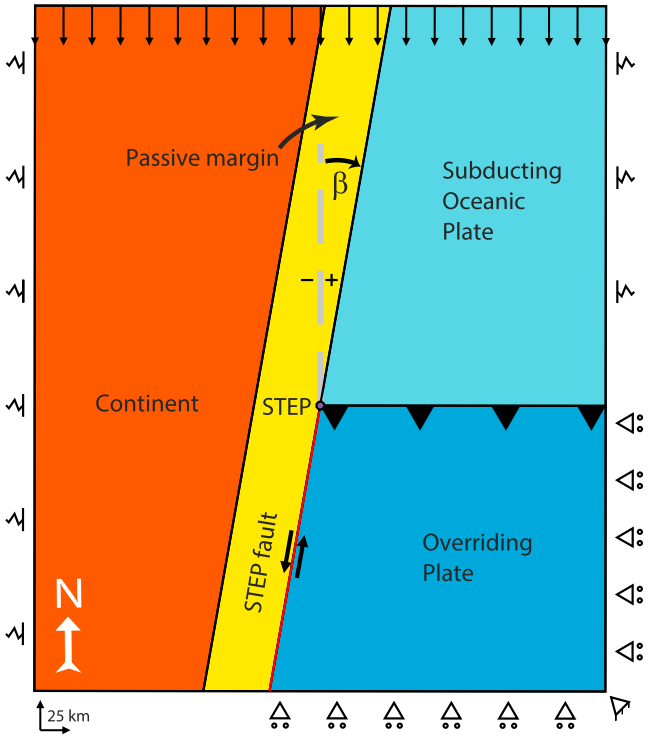

Figure 3. STEP model setup with the STEP (purple hexagon) at the intersection of the subduction fault (trench; with the black dents) and STEP fault (red line, with the two arrows). For reference, we will refer to north, south, east, and west following the arrow in the bottom left. A velocity boundary condition of 1 mm/yr in the N-S direction is set at the northern edge of the model domain. Rollers indicate motion restrictions on the overriding plate. The south-eastern edge cannot move. At the trench, slab pull-associated tractions are forcing the subducting oceanic plate southward. Parameter β represents the passive margin angle. At both sides of the large continental-ocean block, springs indicate lateral continuity of the lithosphere. The southern edge of the continental block is free to move.

We ignore mantle flow contributions to STEP system dynamics in order to determine the effect of material properties on STEP propagation. Slab pull is the driving force for the propagation of a STEP, with continuous subduction and slab rollback as a result. Resistance to tearing at the STEP represents a resisting factor. The mechanical equilibrium equations are solved using the GTECTON finite element software (version 2011.1.65) adopting the plane stress approximation [*Govers and Wortel*, 1999].

3.2. Domain and Regional Geometry

A passive margin is represented as a parallel band between the continental and oceanic domains (Figure 3). *De Franco et al*. [2008] analyze a global 5 min topography data set (ETOPO5) and determine the inclination angles of continental slopes. These authors find that the most common inclination angle from the global distribution is 3°. With a 3000 m vertical drop, the width of the passive margin in the STEP models is thus set to ~57 km.

The passive margin angle β is defined here as the angle between the strike of the passive margin ahead of the STEP fault with respect to a trench-perpendicular setup, where positive angles indicate a "closing" basin, while negative angles indicate an "opening" basin (Figure 3). As slab rollback is progressing and a STEP is propagating along the passive margin, the trench is likely to lengthen along strike in case the passive margin angle β is negative. In case the passive margin angle β is positive, continuous rollback will cause trench shortening along strike of the trench. This also implies that the along-trench dimension of the slab in the mantle (and therefore the distribution of the slab pull to the surface plate) is dependent on this passive margin angle β. Model domain size is set to 500×600 km (Figure 3). After investigating several domain sizes (with a similar grid resolution) we choose this domain size to ensure that model boundaries do not affect STEP propagation (direction).

3.3. Material Properties

England and McKenzie [1982] study continental deformation, assuming no vertical gradient in the horizontal velocity field (strain rate is constant with depth). They show that the average lithospheric strength depends largely on the rheology of the strongest section of the lithosphere. Average lithospheric strength increases with decreasing Moho temperature [*Burov*, 2011].

In a lithospheric plate, different deformation regimes (brittle/elastic/viscous) operate at different time scales and depths, i.e., for specific strain rates and pressure-temperature conditions [*Goetze and Evans*, 1979; *Kohlstedt et al*., 1995; *Ranalli*, 1995; *Burov*, 2011]. Elastic behavior is paramount at short time scales, while brittle and viscous (relaxation and ductile creep) behavior is observed over large time scales [e.g., *Ranalli*, 1995; *Burov*, 2011]. Here we neglect brittle behavior as the brittle layer (only uppermost part of the lithosphere) does not represent the main constituent of lithospheric strength in case the lithosphere is subject

Table 1. Material Properties for Nonuniform STEP Models

Lithospheric Domain	Subducting Plate	Continent	Passive Margin	Overriding Plate
Poisson's ratio (ν)	0.25	0.25	0.32	0.25
Effective viscosity (η)	$1.00\,10^{23}$ Pa s	$0.25\,10^{23}$ Pa s	$0.50\,10^{23}$ Pa s	$0.25\,10^{23}$ Pa s
Young's modulus (E)	75.0 GPa	75.0 GPa	52.9 GPa	75.0 GPa

to strain on the geological time scale [e.g., *England and McKenzie*, 1982; *Ranalli*, 1995]. Using a visco-elastic plate therefore fits our description of the lithosphere. Like *England and McKenzie* [1982], we use a single viscosity for the lithosphere, as a Newtonian fluid. This effective (lithospheric) viscosity represents the average strength of lithospheric plates. We impose a contrast in effective viscosity across the passive margin (1:0.5:0.25, ocean:passive margin:continent; see Table 1). The overriding plate is taken to be relatively weak, resembling either a continental overriding plate or a young oceanic plate that has arisen due to back-arc spreading. Material properties are constant per domain in the model (Table 1). Values for the effective viscosity of the oceanic lithosphere determined from, e.g., geoid modeling and those used in numerical and analog subduction models range from a few times 10^{22} Pa s to 10^{24} Pa s [e.g., *Schellart*, 2004a; *Govers and Wortel*, 2005; *Steinberger and Calderwood*, 2006; *Capitanio et al*., 2009; *Plattner et al*., 2009; *Hale et al*., 2010]. Here we choose to use a value of $1 \cdot 10^{23}$ Pa s for the oceanic lithosphere. For nonuniform models, which include a viscosity contrast, we reduce the shear modulus G of the passive margin by $^1/_3$ to capture the weak, faulted nature of a passive margin.

In order to facilitate the development of a (localized) shear zone, we implement strain weakening of the viscosity:

$$\eta = \eta_{\text{initial}} \cdot \left[a + (1 - a) \exp\left(-\frac{\varepsilon_E^2}{2b^2} \right) \right] \tag{1}$$

where η_{initial} is the initial viscosity (Pa s), η is the new (lowered) viscosity (Pa s), ε_E is the effective shear strain ($\varepsilon_E \equiv \sqrt{1/2\ \varepsilon_{ij}'\ \varepsilon_{ij}'}$ where ε_{ij}' is the deviatoric strain tensor and summation convention is assumed), and a and b are the softening parameters. Parameter a indicates how much the viscosity is weakened in the model, while parameter b controls the interval of effective shear strain ε_E over which weakening occurs. Note that for large effective shear strain (ε_E), $\eta = \eta_{\text{initial}} \cdot a$, the viscosity is weakened maximally in the region of large effective shear strain. In regions where no or little strain is experienced, $\eta = \eta_{\text{initial}}$. Essentially, the function determines the resistance to tearing of the lithosphere, i.e., the ease at which the STEP can propagate.

In the lithosphere, several mechanisms can reduce the strength. In the brittle regime, this involves the formation of faults and fault gouge, which explicitly requires a loss of cohesion and results in a strength reduction by a few percent [*Sibson*, 1977]. In the ductile regime, power law (creep) rheology is acting which is influenced by temperature, pressure, and mineral content [*Goetze and Evans*, 1979; *Kohlstedt et al*., 1995; *Ranalli*, 1995; *Burov*, 2011]. Shear heating [*Regenauer-Lieb and Yuen*, 1998] raises the temperature, altering the power law and possibly inducing mineral transitions. The effect of mineral transitions, especially in the case of pressure solution through water presence, also plays a major role in lithospheric strength reduction [*Kohlstedt et al*., 1995; *Ranalli*, 1995]. For example, the formation of phyllosilicates can reduce the strength by 50–80% [*Bos and Spiers*, 2002]. The role of water is twofold, as pore fluid pressure reduces the dynamic pressure in the system resulting in a decrease of the angle of internal friction. Through these, and probably more weakening mechanisms, we set the effective viscosity to be lowered to 10%, so that a equals 0.1, i.e., a maximum strength reduction of 90%. We set the thickness of all plate domains in the model at 1 m as the actual thickness is already captured in the effective lithospheric viscosity.

3.4. Boundary Conditions

In the numerical models, a low-friction vertical (STEP) fault is implemented with the slippery node technique [*Melosh and Williams*, 1989]. This is indicated by the two black arrows in Figure 3. The subduction fault is also modeled through slippery nodes. Slab pull-associated tractions are acting on the northern side of this internal interface as the transmitted slab pull, forcing this interface south. As these tractions are large in magnitude, motion along the slippery nodes is allowed only in the N-S direction. The STEP (purple hexagon in Figure 3), at the intersection of the subduction and STEP faults, is represented by overlapping full nodes [*Plattner et al*., 2009].

Slab pull is transmitted into the surface part of the subducting plate through the bending area at the trench. In order to capture this transmission into the surface plate, we model a slab and slab pull transmission in a separate model and use the obtained distribution of slab pull-associated tractions in our STEP model. We obtain this distribution by studying the effect of the buoyancy force (through Archimedes' principle) on a slab suspended from the topside (i.e., as at the trench), and we consequently inspect the magnitude of the force needed to keep the topside in place. A further description of the determination of the slab pull-associated tractions is made in Appendix A. The main notion from these models is the effect of the orientation of the passive margin with respect to the trench (β in Figure 3), i.e., the slab shape in the upper mantle, on the slab pull-associated tractions. These are largest near a STEP and show a 1/r behavior along trench, decreasing away from the STEP (see Figure A2). In a subduction system, several resisting forces act on the slab, including deep mantle resistance at the downdip tip of the slab, mantle (viscous) drag on the sides of the slab, compositional buoyancy within the slab, and friction along the plate contact zone. We capture these resisting forces using a reduction factor, which decreases the magnitude of the slab pull-associated tractions transmitted into the surface plate.

The springs in Figure 3 represent Winkler pressures. Winkler pressures are essentially spring boundary conditions: a resistance to motion perpendicular to the boundary is set through a spring constant. On an atomic scale, resistance to compression is acting through the atomic bonds, which can be considered little springs. On a rock sample (and lithospheric) scale, this resistance is defined as the bulk modulus: a measure for the resistance against uniform compression. Therefore, the bulk modulus K is set as spring constant. As Winkler pressures are applied at the lateral boundaries of the continental-subducting ocean block, it represents the notion of lateral continuity of lithosphere with the same material properties (as this material outside the model domain will have the same bulk modulus). The overriding plate is constrained at its southern edge in the N-S direction and at its eastern edge in the E-W direction. This resembles continuity of the N-S velocity across the eastern edge of the overriding plate and essentially indicates continuity of the overriding plate in the east direction.

As the goal of these models is not to represent a specific, natural setting, we set a velocity boundary condition of 1 mm/yr in the N-S direction at the northern side. The E-W component is left free. This velocity may be too small for direct comparison with processes on a geological scale, but it ensures that the combined effect of a STEP setting with the inclusion of a passive margin and the slab pull transmission at the trench can be clearly observed. The southern edge of the continental block is free, and movement along the STEP fault is frictionless. It is also assumed that the subduction fault is well developed. We test the effect of changing boundary conditions, including the magnitude of the velocity at the northern boundary and the effect of friction along the STEP fault in Figures S1–S5 in the supporting information.

The Maxwell time τ is defined as $\tau \equiv \eta/\mu$, where η is the lithospheric viscosity and μ is the shear modulus. It represents the characteristic relaxation time for the model. Model results are shown for a model time of 1.057 Ma, corresponding to 100 τ of the maximally weakened, subducting oceanic plate. In this way, results for this model setup show a near-instantaneous response to boundary conditions. All model results depicted in the following have converged; i.e., results do not change when decreasing the mesh or time step size.

4. Uniform Mechanical Properties

4.1. Model Results

We first study a geometry similar to the models of *Govers and Wortel* [2005] to confirm whether the first-order response of STEP settings is indeed approximately STEP fault parallel. In Figure 4, model results for a uniform model are depicted where the trench and STEP fault are oriented perpendicular. Neither strain weakening of the viscosity nor a viscosity contrast is implemented, in accordance with *Govers and Wortel* [2005]. Black lines in Figure 4 indicate the trace of the different domains (only plotted for easy comparison with subsequent results which do include viscosity contrasts and viscosity weakening).

In Figure 4, the effect of the subduction-transform transition and slab pull-associated tractions is shown in the direct vicinity of the STEP through the effective shear strain. The strain buildup at the STEP is oriented at an angle of ~80° with respect to the trench. Velocity vectors in the total displacement plot indicate an increase in magnitude toward the trench from the north side of the model. A horizontal component is present, resulting

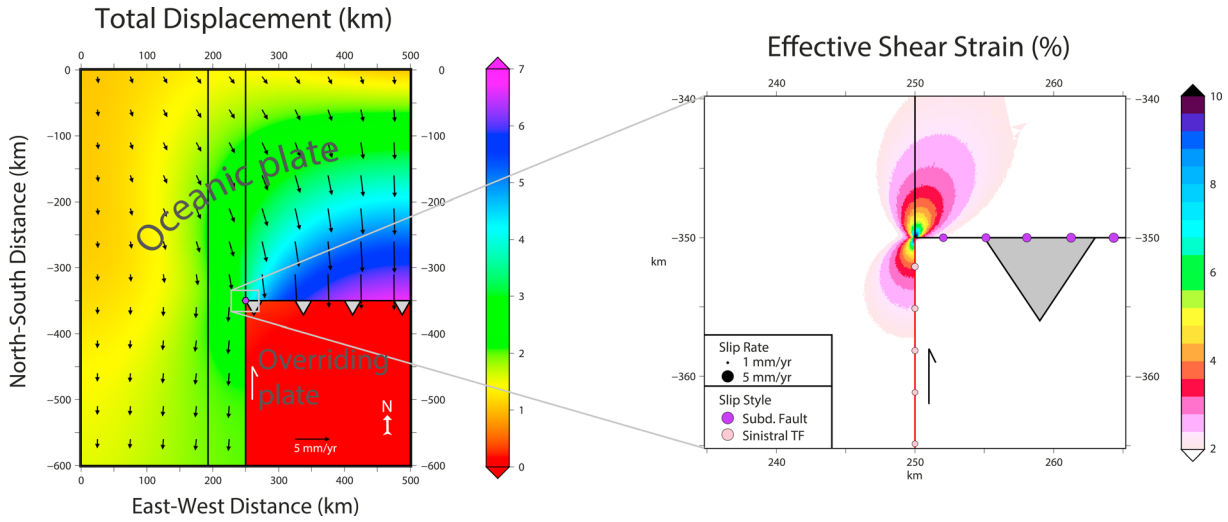

Figure 4. Model results for the uniform model. Contour plots show the (left) total displacement (km) and (right) effective shear strain (%). The effective shear strain plot shows the area directly around the STEP, while the displacement plot shows the results for the whole model. In the displacement plot, velocity vectors are included for the surface-subducting (oceanic) plate block. The grey dents indicate subduction direction, and slip symbol shows the sinistral character of the STEP fault (red line). Slip rates along the faults are shown through two colored circles whose size depends on the magnitude of the slip rate. The active STEP is indicated through a magenta hexagon in the displacement plot.

in a motion of the western side of the subducting plate toward the trench. South of the STEP, indicated with the magenta hexagon, the block shows rather uniform motion. Overriding plate motion is negligible for this uniform model setup. The total displacement plot indicates that displacement increases toward the trench, while it remains quite constant along the left-lateral side of the model domain. Slip along the STEP fault is nonuniform, and differential slip across the trench increases away from the STEP. Even though forcing is largest near the STEP (green line in Figure A2), the largest displacements are observed at large distances from the STEP, toward the easternmost model boundary.

4.2. Sensitivity and Analysis for Uniform Model Results

The STEP acts as a drag point, where displacement decreases and a buildup of strain occurs. The concentration of shear strain north of the STEP, as depicted in Figure 4, indicates the formation of a shear zone which allows the STEP to propagate. The concentration south of the STEP is a result of the compressional stress and shows that the lithosphere in the wake of the STEP is still being damaged as a result of STEP propagation. Velocity vectors increase away from the STEP along trench, but this does not necessarily indicate a rotating trench. As the velocity vectors are almost equal in magnitude and direction onward from about 150 km from the STEP, it indicates that a more concave (toward the mantle wedge side) geometry will arise as rollback continues. This fits our notion of high resistance to tearing in case little (or none, as in this setup) strain weakening of the viscosity is implemented which results in a curvature of the trench as rollback continues.

In our model setup, as discussed in the model setup section, we make several assumptions regarding boundary conditions, plate viscosity, and friction along the STEP fault. We investigate the effect these assumptions have on the ensuing STEP propagation direction in Figures S1–S5. We show there the results for one model geometry and a range of model assumptions, including the prescribed plate velocities, strain viscosity weakening parameter a, and reducing factor of the slab pull-associated tractions. We emphasize that the observed (in) sensitivity to our model assumptions is representative for all models we present in this study.

At the lateral sides of the model domain in Figure 4, the velocity vectors are oriented parallel to the model domain side. It can be concluded that Winkler pressures resemble symmetry boundary conditions: the N-S velocity is continuous across the edge of the model domain. The magnitude of the velocity boundary condition at the northern edge of the model domain is set at 1 mm/yr for the depicted model results. Results of models with different velocity magnitudes, different velocity orientations, and velocities on other boundaries besides the northern boundary (not shown here) indicate that only the displacement field is altered with respect to the results of Figure 4. Strain buildup north of the STEP is oriented in the same direction with only

minute changes in the extent of the lobe. This is an indication that the STEP propagation direction does not depend on prescribed plate velocities.

In case we add friction along the STEP fault, up to the point of essentially locking the fault, we also do not observe a change in the STEP propagation direction (Figure S3). In the current model setup, differential motion across the trench is allowed only in the N-S direction. In case this constraint is omitted and oblique subduction is allowed, differential motion is still dominated by the N-S component. The maximum deviation from this N-S orientation is only ~6°. Just as the change in magnitude of the velocity boundary condition at the northern side of the model domain, the orientation of the effective shear strain buildup does not change when relaxing this differential motion constraint. Therefore, it appears that the formation (and especially the orientation) of a shear strain zone north of the STEP is not affected on a large scale by model boundary conditions.

Slab forcing at the trench represents a factor influencing the displacement field as well as the shear zone formation north of the STEP. Reducing the magnitude of the slab pull-associated tractions, e.g., by reducing the slab dip, also reduces the amount of shear strain concentration north of the STEP. However, the orientation is not altered. It appears that the slab pull-associated tractions acting at the trench are the dominating factor for the model results, with a large increase in both the velocity and displacement fields toward the trench. This increase in velocities and displacements toward the trench becomes less and less significant for increasing boundary velocity magnitudes, while not affecting the STEP propagation direction.

We conclude that the ensuing STEP propagation direction is not affected by surface plate velocities and completely depends on the presence of a considerable forcing across the trench. Model displacements show different magnitudes for different velocity boundary conditions, but the gradients of displacement at the STEP are similar. Shear stresses and strains arising due to the sudden disruption of slab pull transmission at the lateral edge of the subduction zone, i.e., at the STEP, are therefore also similar, causing a corresponding orientation of the arising shear zone.

The buildup of effective shear strain indicates the formation of a shear zone at an ~10° angle to the STEP fault-parallel direction. Propagation of the STEP for this uniform model will thus not be in an exact N-S direction. However, this ~10° angle still fits the approximately STEP fault-parallel orientation of *Govers and Wortel* [2005].

5. Straight Passive Margin

5.1. Model Results

In the previous section, we determined that for uniform models, i.e., where a completely oceanic lithosphere is part of the subduction system, the STEP propagates approximately perpendicular to the trench (STEP fault parallel), in accordance with the findings of *Govers and Wortel* [2005]. Now we will determine the effect of a viscosity contrast on the propagation direction in case a passive margin is involved in the geodynamic setting. This is done for a range of β, with the viscosity contrast as described in the model setup section (1:0.5:0.25, from ocean to continent across the passive margin) and strain weakening of the viscosity. Per model setup we use a forcing calculated for the corresponding mantle slab shape (Appendix A). Results are depicted in Figure 5. Note that the two rows, both for the effective shear strain and total displacement plots, have different maximum values for the color-scale bars.

Model results for $\beta = 0$ are depicted in the left column of Figure 5, and a quick comparison with the results of Figure 4 provides evidence for some essential differences. Strain weakening of the viscosity results in a large-strain buildup along the passive margin-subducting ocean interface inside the passive margin. Velocity vectors indicate an increase in magnitude toward the trench, and the overall velocity magnitudes are larger than for the uniform viscosity model.

For models where $\beta = 30°$ in the positive quadrant, so that the trench is likely to shorten as rollback continues (see Figure 3 for positive and negative quadrants), a different behavior of the STEP is observed as can be seen in Figure 5. Compared to the case where $\beta = 0$, a larger increase in magnitude of the velocity vectors toward the trench is visible. Also, the total displacement reaches higher values. The horizontal component of the velocity is larger than for the previously depicted model results. Differential slip across the subduction fault is largest near the STEP and decreases away toward the east, in correspondence with the forcing at the trench through the slab pull-associated tractions (Figure A2).

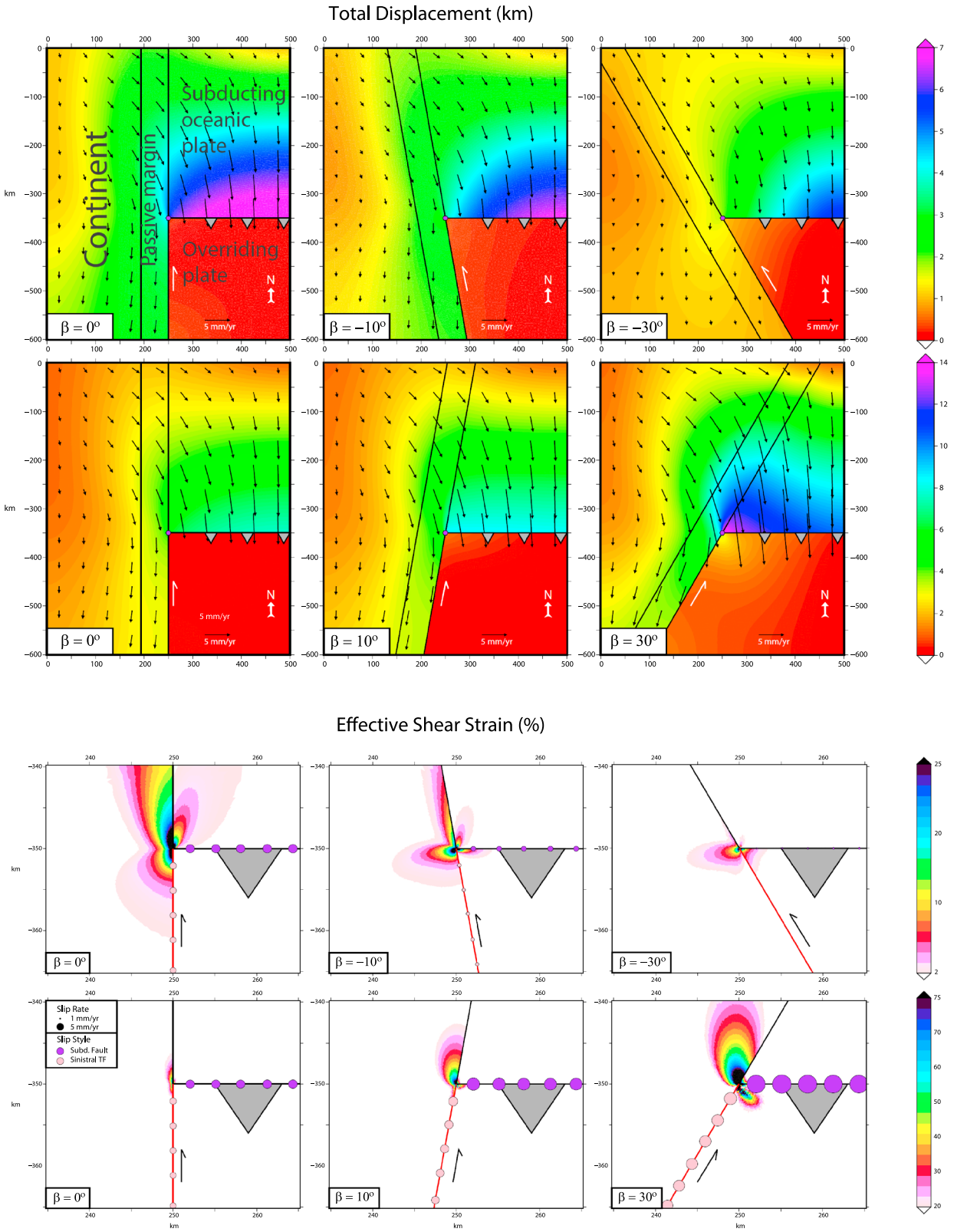

Figure 5. Model results for a range of β. The contour plots show the total displacement and effective shear strain. The effective shear strain plots show the area directly around the STEP, while the total displacement plots show the results for the whole models. In the displacement plots, velocity vectors are included for the surface-subducting plate block. The grey dents indicate the subduction direction, and the white slip symbol indicates sinistral nature of the STEP fault. For models where β equals −30, −10, 0, 10, and 30, b equals 0.008, 0.02, 0.02, 0.02, and 0.05, respectively. Scale bars are constant per row. Slip rate magnitudes are the same as in Figure 4.

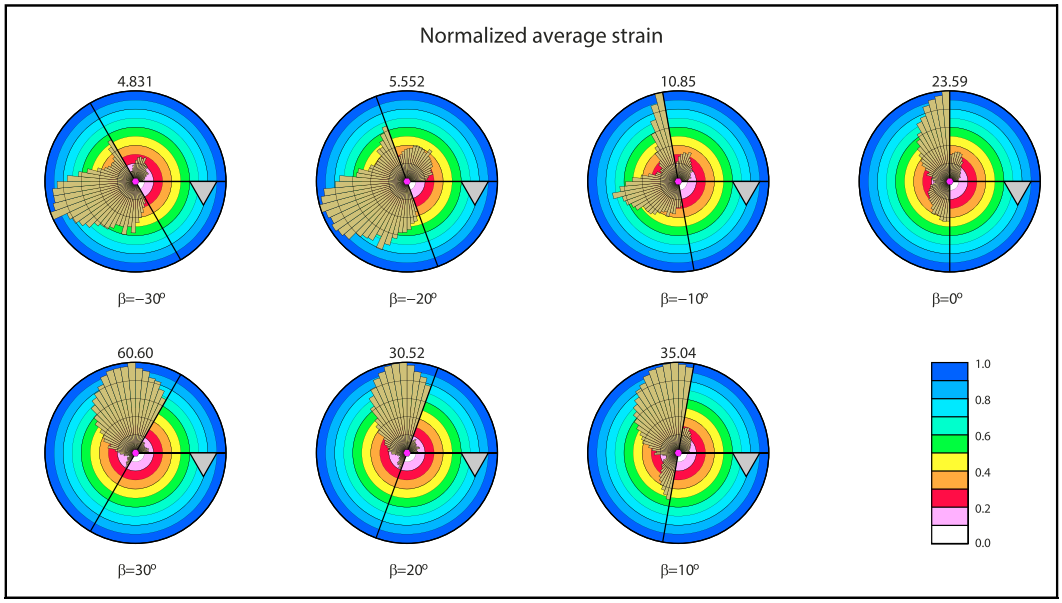

Figure 6. Pie charts of the normalized average strain within the first 10 km surrounding STEPs for a range of models with different β and straight passive margins. The grey dents indicate subduction direction, and the magenta hexagons represent the STEP. Every pie chart is normalized by the largest value of the average (effective shear) strain contained by a pie wedge (number above pie chart). Color scale emphasizes this normalization. The black lines represent passive margin orientation.

When the passive margin angle β is negative, a different behavior is observed at the STEP. For a model with an angle β of $-10°$, the light blue line for forcing in Figure A2 is implemented. Figure 5 shows that a buildup of effective shear strain occurs parallel to the STEP fault, inside the passive margin. However, when compared to the above-mentioned results, another shear strain concentration arises parallel to the trench. Effective shear strain and principal stress magnitudes are much lower compared to a model with a passive margin angle in the positive quadrant.

In case the passive margin angle is even more negative ($\beta = -30°$), the model setup results in an even more oblique subduction with respect to the passive margin. Forcing at the trench diminishes further (dark yellow line in Figure A2), and the resulting effective shear strain and total displacement plots in Figure 5 indicate that determining the propagation direction for the STEP is a difficult exercise. The increase in the magnitude of the velocity field at the subducting plate and resulting displacements do not cause large-scale deformation patterns. Magnitudes of the principal stresses do no reach high values. A small compressive shear zone arises parallel to the STEP. Slip rates across the trench increase significantly away from the STEP along trench.

5.2. Analysis

In case $\beta = 0°$, the active STEP semidecouples the oceanic subducting plate from the continental surface part, with a larger increase of the N-S component of the displacement toward the trench compared to a uniform subducting surface plate (Figure 4). For this model setup, it is clear that a STEP will propagate toward the north along the passive margin-ocean interface. It must be noted that the buildup of strain inside the passive margin is not merely a result of strain weakening of the viscosity: a model without strain weakening shows a similar buildup of strain, but with strain weakening, the lobe of effective shear strain is more pronounced.

A quantitative display of the relative importance of particular STEP propagation directions is shown in Figure 6. Here a collection of pie charts is presented which show the normalized average (effective shear) strain within the first 10 km from the STEP, per 5° slices. Per 5° bin, the average effective shear strain is calculated. Per pie chart, all average values are subsequently normalized by the largest value of a slice in that chart (number above the pie chart). These charts highlight the relative importance of the effective shear strain lobes and therefore provide a means to discriminate between the (possible) propagation directions of the STEP for a range of β. In this way, we present an easy comparison between different model setups. Note that the amount of strain observed in the different models is not identical (as in Figure 5).

Due to a large forcing at the trench (increasing toward the STEP) used in this model setup (red line in Figure A2), a model where $\beta = 30°$ displays an increase in the slip rates toward the STEP. As the STEP fault is modeled here as a transform fault, the N-S motion of the continental-oceanic block needs to be partitioned. Therefore, the edge of the overriding plate is pushed southward at the STEP. The STEP will propagate straight to the north for this model setup, into the passive margin, as confirmed by the pie chart in Figure 6 with the largest peaks straight to the north. The buildup of large strain results in a semidecoupling of the subducting plate and the continental part of the block, which means that as rollback continues, the passive margin will be subducted too. However, as the velocity vectors across the trench indicate a rotation of the trench toward a more perpendicular setup, it is unlikely that the continental material will be pulled into the subduction zone as the trench will rotate. We therefore expect the system to evolve toward a perpendicular trench-margin geometry.

For models with $\beta = -10°$, the low amount of effective shear strain and differential stress compared to the above-mentioned models is due to lower values of the slab pull-associated tractions. Again, the N-S motion of the continental-subducting ocean block needs to be decomposed at the STEP fault. The STEP causes a large resistance to the southward movement, and a compression zone arises. Besides this zone of compression, another shear zone which arises along the passive margin will result in a clear propagation of the STEP as its pie chart (Figure 6) indicates that the amount of strain in this peak along the passive margin-ocean boundary is larger than in the compression zone.

If the passive margin angle β is $-30°$, the total amount of strain in the model has decreased even further (Figure 5). The small concentration of effective shear strain parallel to the trench does not represent a propagating STEP, and differential stress values are not high enough to result in tearing of a lithospheric plate (Figure 6). The large increase in slip rates across the trench away from the STEP provides evidence that the trench will rotate toward a more perpendicular setting for trench and passive margin.

Changing the magnitude of the viscosity contrast across the passive margin does not have a large effect on the STEP propagation direction (Appendix B). Only the amount of strain observed in the passive margin changes. The direction of strain localization, i.e., the STEP propagation direction, does not change. Therefore, we conclude that the magnitude of the viscosity contrast (and the strength contrast) across the passive margin does not affect the propagation direction of a STEP.

It is clear from the distribution of displacements throughout the model and development of effective shear strain lobes at the STEP that the forcing at the trench is the dominating factor. Just as for the uniform subducting surface plate (Figure 4), we do not observe any change in the STEP propagation direction in case we change the magnitude of the forcing (slab pull-associated tractions) at the trench (Figure S4). When reducing the magnitude of the forcing, the magnitude of the effective shear strain is also reduced, but the orientation of the lobe does not change. As for the uniform model, changing the magnitude and orientation of the prescribed velocities at the model boundaries does not alter the described STEP propagation directions (Figure S1).

The passive margin width for the generic models is set at ~57 km, based on the results of *De Franco et al.* [2008]. Several model results indicate that a modification of this width does not have a large influence on the localization of effective shear strain and the resulting radiation pattern (Figure S2). Effective shear strain buildup is still concentrated at the passive margin-ocean interface. Also, the viscosity contrast across the passive margin does not have a large influence on the propagation direction of a STEP. For example, in case the viscosity contrast is set in 10 steps instead of three, so that eight parallel bands, with one effective viscosity per band and a constant jump in viscosity across each interface, are present in the passive margin, strain localization takes place along the first material property contrast near the STEP. The magnitude of this contrast, whether increased or lowered, does not influence the orientation of the effective shear strain buildup. These observations indicate that smaller-scale details of the model setup are not key parameters: only the orientation of some contrast in material properties and a considerable forcing are necessary to change the STEP evolution behavior.

Even though the passive margin guides STEP propagation, resistance to tearing is still a factor causing curvature of the trench. Therefore, we need to determine whether the observed behavior for a 90% strength reduction, as in the presented model results, is exemplary for STEP propagation behavior. When increasing the maximum strength reduction from 90% to 99%, i.e., changing a in equation (1) from 0.1 to 0.01, we observe some slight differences in the effective shear strain lobe in models (Figure S5). As the lithospheric plate only retains 1% of

its original strength in the region of maximum effective shear strain, the localization of deformation is enhanced. In cases ($\beta > -15°$) where the STEP is either tracking or propagating into the passive margin, enhanced localization and therefore a raised level of effective shear strain is present, but there is no change in the propagation direction. For models with $\beta \approx -15°$, the STEP propagation direction remains difficult to determine.

In case the passive margin angle lies within 15° of the "stable" perpendicular setup, a STEP will propagate readily along the passive margin-ocean interface. In case this angle lies in the negative quadrant, a shear compression zone arises parallel to the trench in the passive margin. When it exceeds this 15° difference (in the negative quadrant), only this shear compression zone is present and there is no clear indication for STEP propagation. This basically slows down the progress in the STEP system evolution: only when the trench has retreated further, with a rotation toward orthogonality as determined from the slip rates (increase away from the STEP), the STEP can propagate further as the system is again in the stable window of STEP propagation. This implies that the friction at the STEP causes the STEP to act as a pivot around which the trench can reorganize toward orthogonality. Propagation occurs straight into the passive margin when β exceeds 15° in the positive quadrant. This will result in more localized strain in the weak passive margin which in first instance will result in higher rollback rates toward the STEP. A rotation toward orthogonality is the logical result.

We can thus conclude that, even though there is a stable window for which STEPs propagate readily along a passive margin, a setup outside this window has the tendency to evolve toward a perpendicular geometry. For small ($<10°$) changes in the passive margin angle, model results show similar behavior, indicating that the model setup is relatively insensitive to small-scale details. The influence of crustal-scale heterogeneities is thus quasi-inexistent compared with the large stresses producing the tearing of the lithosphere by slab pull.

6. Changes in the Orientation of Passive Margins

6.1. Numerical Model Approach

Passive margins are commonly not straight. A present-day situation where a passive margin changes orientation ahead from the STEP, is the southern termination of the south Lesser Antilles subduction zone (Figure 2 and Figure 7a). At some point in the rollback evolution, a change in passive margin strike will occur, and we will determine what the behavior of a propagating STEP will be when approaching and passing such a kink. Figure 7a depicts the southern part of the south Lesser Antilles subduction zone, where the passive margin ahead of the active STEP is oriented at a kink with respect to the edge of the continental margin along which the STEP has propagated since ~45 Ma [*van Benthem et al.*, 2013]. We investigate models which include such a kink in passive margin strike, both abrupt (solid passive margin-ocean line in Figure 7b) and gradual, i.e., with a radius of curvature (dotted and dashed lines in Figure 7b).

In essence, the model setup where the active STEP encounters an orientation change of the passive margin, is equal to that of the straight passive margins in the previous section. We use the green line of Figure A2 for the forcing at the trench for all models. For the models studied in this section, a model setup is shown in Figure 7b. The passive margin has a change in strike at the STEP, representing a situation where the STEP has propagated along the passive margin up to this kink. Again, the plates are modeled with the same viscosity contrast used in the previous section (1:0.5:0.25, from subducting ocean to continent, across the passive margin).

To discriminate between model setups with a straight passive margin, the "kink passive margin angle" β_k represents the angle of the passive margin ahead of the STEP with respect to a trench-perpendicular setup in the subsequent models. Here we will also determine over which distance the "abrupt behavior" is observed and when a change in behavior occurs. We first discuss results and implications for models with an abrupt change in orientation of the passive margin. Such an orientation change can also be made through a radius of curvature. We will only study models in the range where no direct propagation along the passive margin is observed and the effect of a radius of curvature is likely to result in different STEP behavior.

6.2. Model Results for a Kink in Passive Margin Strike β_k

In Figure 8, the results are depicted for models with a range of β_k and an abrupt kink. For models where the passive margin angle β_k is very negative ($<-45°$); i.e., the passive margin is "rotating away" very obliquely from the trench, a buildup of effective shear strain arises inside the subducting oceanic basin. Differential stress concentrates in this same area. There is no considerable effective shear strain concentration observed in the passive margin, and slip rates across the trench are relatively low compared to other model setups. These

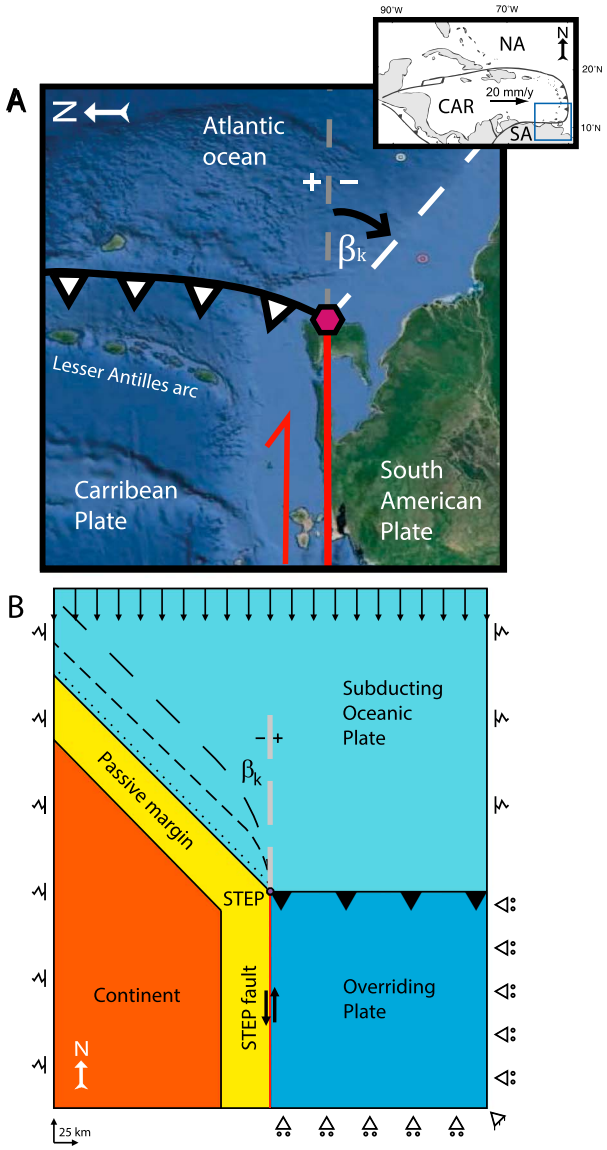

Figure 7. (a) Setting of the south Lesser Antilles subduction zone in the Caribbean. As for Figure 3, the white dashed line indicates the extent of the passive margin ahead of the STEP (purple hexagon). The trench indicated here with the black dents depicts the end of the subduction contact zone, distinctly different from the conventional use of the trench definition. The grey dashed line shows the trench-perpendicular orientation, so that the kink passive margin angle β_k is the angle difference between the grey and white dashed lines. The north arrow indicates geographic north. (b) STEP model setup with the STEP (purple hexagon) at the intersection of the subduction fault (trench; with the black dents) and STEP fault (red line, with the two arrows). For reference, we will refer to north, south, east, and west following the arrow in the bottom left. A velocity boundary condition in the N-S direction is set at the northern edge of the model domain. Rollers indicate motion restrictions on the overriding plate. The south-eastern edge cannot move. At the trench, slab pull-associated tractions are forcing the subducting oceanic plate southward. Parameter β_k represents the kink passive margin angle. The dotted and dashed lines indicate several gradual changes in passive margin strike. At both sides of the large continental-ocean block, springs indicate lateral continuity of the lithosphere. The southern edge of the continental block is free to move.

show similar magnitudes onward from ~150 km along trench from the STEP. Both the displacement and velocity fields increase toward the trench.

In model setups where β_k is approaching values of ~−25°, a buildup of the effective shear strain arises along the passive margin-ocean interface, but a concentration of strain is also present inside the subducting oceanic plate. In case β_k is between −15° and 15°, a large concentration of effective shear strain is present alongside the passive margin-ocean boundary. Model results are rather similar, with an increase in both the displacement and velocity fields toward the trench and the notion that slip rates across the trench show the same magnitudes onward from ~150 km along trench from the STEP.

As β_k exceeds values of ~20°, the model results show a different behavior. A large strain concentration arises inside the passive margin, not clearly following the passive margin-ocean boundary but rather oriented (sub) perpendicular to the trench. The displacement and velocity fields show a larger increase in magnitude toward the trench, and slip rates are now largest near the STEP and decrease away along trench. This is in contrast with the above-mentioned model results. This is a similar result as for the straight passive margins with $\beta > 10°$.

6.3. Analysis of Kinked Margin Models

In case β_k is smaller than ~−30°, the sole lobe of effective shear strain is an indication that the STEP will propagate into the ocean basin. This is emphasized in Figure 9, where several pie charts for the normalized average strain are presented (as for Figure 6). These pie charts show that for $\beta_k < -30°$, the STEP will propagate into the oceanic basin. It appears that for such angle β_k, the gap toward the passive margin is simply too large bridge. The direction of STEP propagation is subperpendicular to the trench.

For $\beta_k = -30°$, the largest peak is located inside the passive margin, but

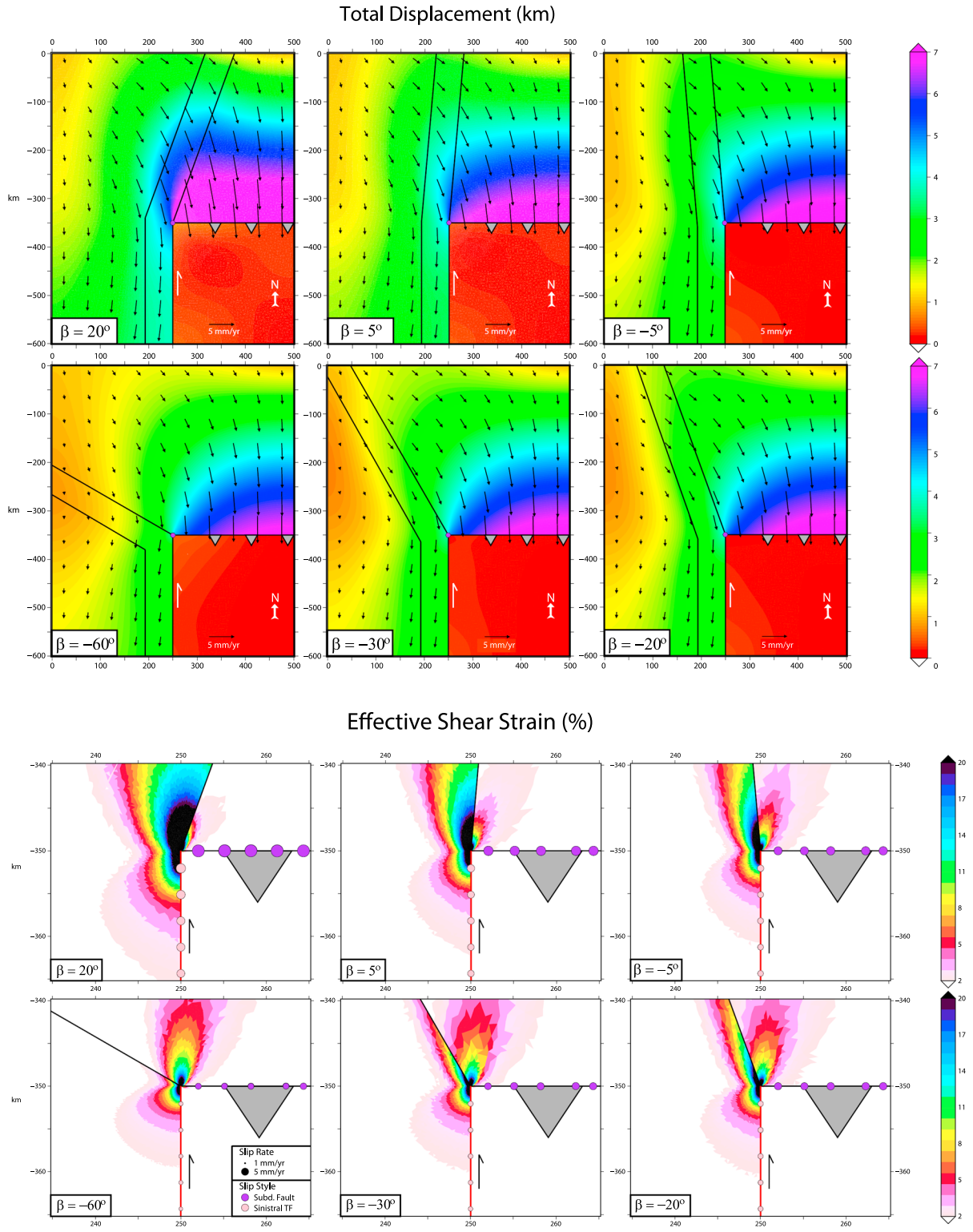

Figure 8. Model results for a range of β_k. The contour plots show the (top rows) total displacement and (bottom rows) effective shear strain. The effective shear strain plots show the area directly around the STEP, while total displacement plots show the results for the whole models. In the displacement plots, velocity vectors are included for the surface-subducting plate block. The grey dents indicate the subduction direction, and the white slip symbol indicates the sinistral nature of the STEP fault. For all models, *b* equals 0.02. Scale bars are constant per row. Slip rate magnitudes are the same as in Figure 4.

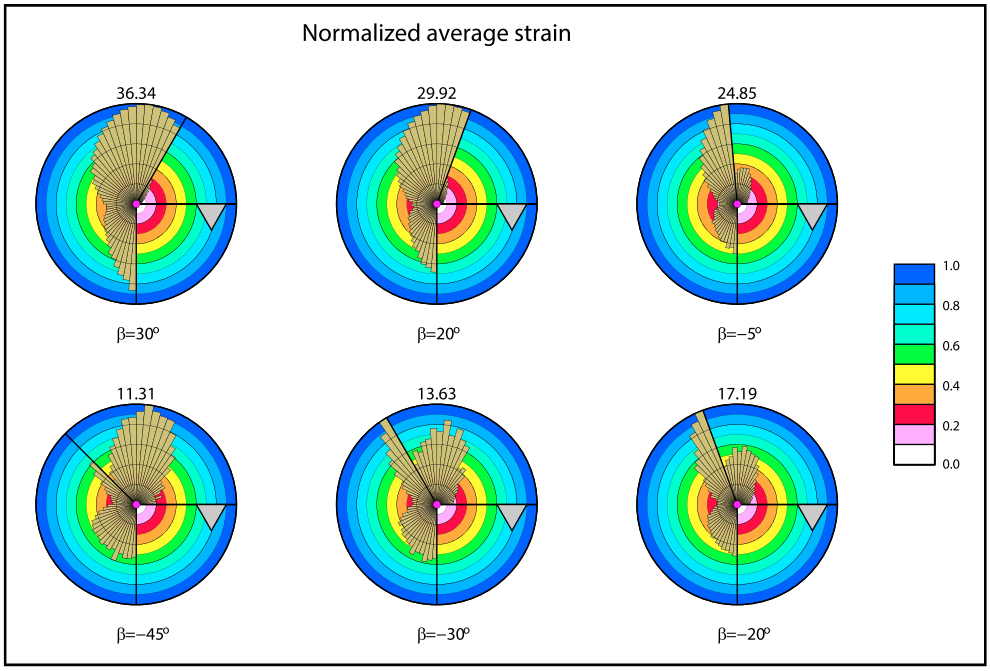

Figure 9. Pie charts of the normalized average strain within the first 10 km surrounding STEPs for a range of models with different β_k and kinked passive margins. The grey dents indicate subduction direction, and the magenta hexagons represent the STEP. Every pie chart is normalized by the largest value of the average (effective shear) strain contained by a pie wedge (number above pie chart). Color scale emphasizes this normalization. The black lines represent the passive margin orientation.

the amount of strain inside the oceanic domain is quite considerable and determining the actual propagation direction is difficult. This setup represents a transition between a situation where the STEP is propagating into the oceanic basin, and one where it is following the passive margin. Propagation depends directly on the strength of the passive margin and subducting plate. In a geodynamic situation where a strong and cold oceanic plate is subducting, the strength may be high enough to compel STEP propagation along the passive margin-ocean interface. In the situation of a relatively weak subducting plate, the STEP may well propagate straight into the oceanic plate. This "transition orientation" ends at $\beta_k = -20°$, where strain is clearly largest inside the passive margin (Figures 8 and 9).

The STEP will propagate along the passive margin-ocean boundary for setups where β_k is between $-25°$ and 25°. This appears to be a stable setup. Just as for straight passive margins, adding friction to the STEP fault, up to the point of essentially locking the STEP fault, does not cause the STEP to propagate in a different direction. This shows that the nature of the lithosphere south of the STEP does not influence STEP propagation (direction), and it also suggests that, in case a trench is retreating obliquely toward a passive margin, a STEP can be captured by a passive margin if the strike of the passive margin is within 25° of a trench-perpendicular setup. In case β_k is between 15° and 25°, the oblique orientation of the passive margin results in a strong shear zone so that subducting plate velocities increase toward the STEP. This indicates that a trench will rotate back toward a stable perpendicular setup. As for model setups with straight passive margins, small ($<10°$) changes in the angle β_k do not result in different propagation behavior for the STEPs. This is a confirmation that the STEP model setup is relatively insensitive for short-wavelength geometric changes.

As for the straight passive margin models, we observe some slight differences in the STEP propagation direction for models (not shown here) in case we allow for further strength reduction in the area of high effective shear strain. In case $\beta > -25°$, the STEP will continue to either track or propagate into the passive margin, with a more localized deformation lobe which includes higher values for the effective shear strain. For models where the STEP does not track the passive margin, but rather propagates into the oceanic basin, we observe a slightly different behavior. Close to the STEP, the effective shear strain lobe is oriented more trench perpendicular. Further away from the STEP, it turns toward the same orientation as for larger values for a (in equation (1), i.e., in case of

less strength reduction). This is an indication that a STEP will propagate in a trench-perpendicular fashion in case the resistance to tearing is very low, while a STEP will propagate slightly subperpendicular (~80° from the trench) in case of higher resistance to tearing.

The results presented in Figure 9 do not explicitly mean that a STEP cannot propagate when the passive margin is oriented with a large angle from the stable perpendicular position. It is possible that a large change in orientation is not made in one kink but rather is distributed over a larger distance as displayed in the model setups in Figure 7b. We will now determine what the influence of a change in strike of a passive margin through a radius of curvature instead of an abrupt kink is on the STEP propagation direction.

6.4. Results for a Gradual Change in Passive Margin Strike β_k, an Evolution Series

We now study gradual kink models with those kink passive margin angles for which the abrupt kink models resulted in STEP propagation into the oceanic basin. Setups with angles which already show STEPs tracking an abruptly kinked passive margin will not be influenced by such a gradual kink in the passive margin. To determine the effect of a gradual kink on STEP propagation, we first study a setup which includes a very gradual change in strike. Note here that we do not use perfectly curved sides of elements at the passive margin-ocean interface but the gradual change in passive margin strike is obtained through a series of small (2.5°) steps in orientation. This may cause some additional model-induced strain. The model domain size is varied throughout the evolution series to retain a 250 km-to-the-west-side distance for the STEP and a 350 km-to-the-north-side distance for the trench as for all the previous model setups.

We will now discuss an evolution series to show the behavior of STEP propagation direction and rollback evolution as determined from our model results. This evolution, with the reorganization of the trench and redirectioning of the slab pull-associated tractions, is derived from the model results of every previous time step. Slip across the trench is determined and is represented in the new model setup in a stylized manner: we assume that this is the rollback pattern of the trench and that it remains perpendicular to the passive margin while a stylized line ensures that we avoid the effect of model-induced strain. Throughout the evolution, we keep a constant magnitude of the slab pull-associated tractions acting at the trench. By assuming that the slab dip does not change, the slab was already reaching the mantle transition zone, and the slab follows the shape of the trench, we consider that the portion of the slab perpendicular to the trench (and thus the slab pull force) remains constant.

In Figure 10, we present such a model evolution which exhibits a gradual change in passive margin strike of 60° through a radius of curvature of ~220 km. At the starting model setup (top row in Figure 10), the STEP propagation direction is simply determined from the effective shear strain and normalized average strain plots, i.e., along the passive margin-ocean interface toward the north. As for the model with $\beta = 0$ in Figure 5, i.e., where a straight passive margin is oriented perpendicular to the trench, slip across the trench increases away from the trench.

From this we determine the subsequent (stylized) location of the trench at the second time step (second row in Figure 10). Here the STEP has propagated along the passive margin, but most of the trench has retreated further, resulting in a concave geometry toward the mantle wedge side. As the (mainly) N-S motion in this area is not decomposed well at the STEP fault, partly due to the imperfect model geometry, displacements and velocities at the overriding plate indicate that, near the STEP, the overriding plate is dragged southward. Also, the magnitudes of the displacements diminish near the original location of the STEP (at 250; −350 in Figure 10), which also represents the intersection of the oblique and N-S oriented parts of the STEP fault. This is also probably due to the imperfect model geometry. Slip across the trench and along the STEP fault are both smaller in magnitude compared to the previous time step. Again, STEP propagation is oriented along the passive margin. The trench in this model setup has already lengthened a little, as can be determined from the extra space in between the two grey triangles to the left in the displacement plot. This lengthening of the trench slowly induces the formation of an amphitheatre-shaped slab.

In the two subsequent time steps, the STEP has propagated further along the passive margin and the amount of slip across the trench has slightly diminished further toward the STEP. This results in a longer segment of the trench which is oriented perpendicular to the passive margin, while only a continually smaller section remains parallel to the original trench orientation. Strain localization favors STEP propagation along the passive margin-ocean interface, even though the model at the fourth row shows an increase in the dragging

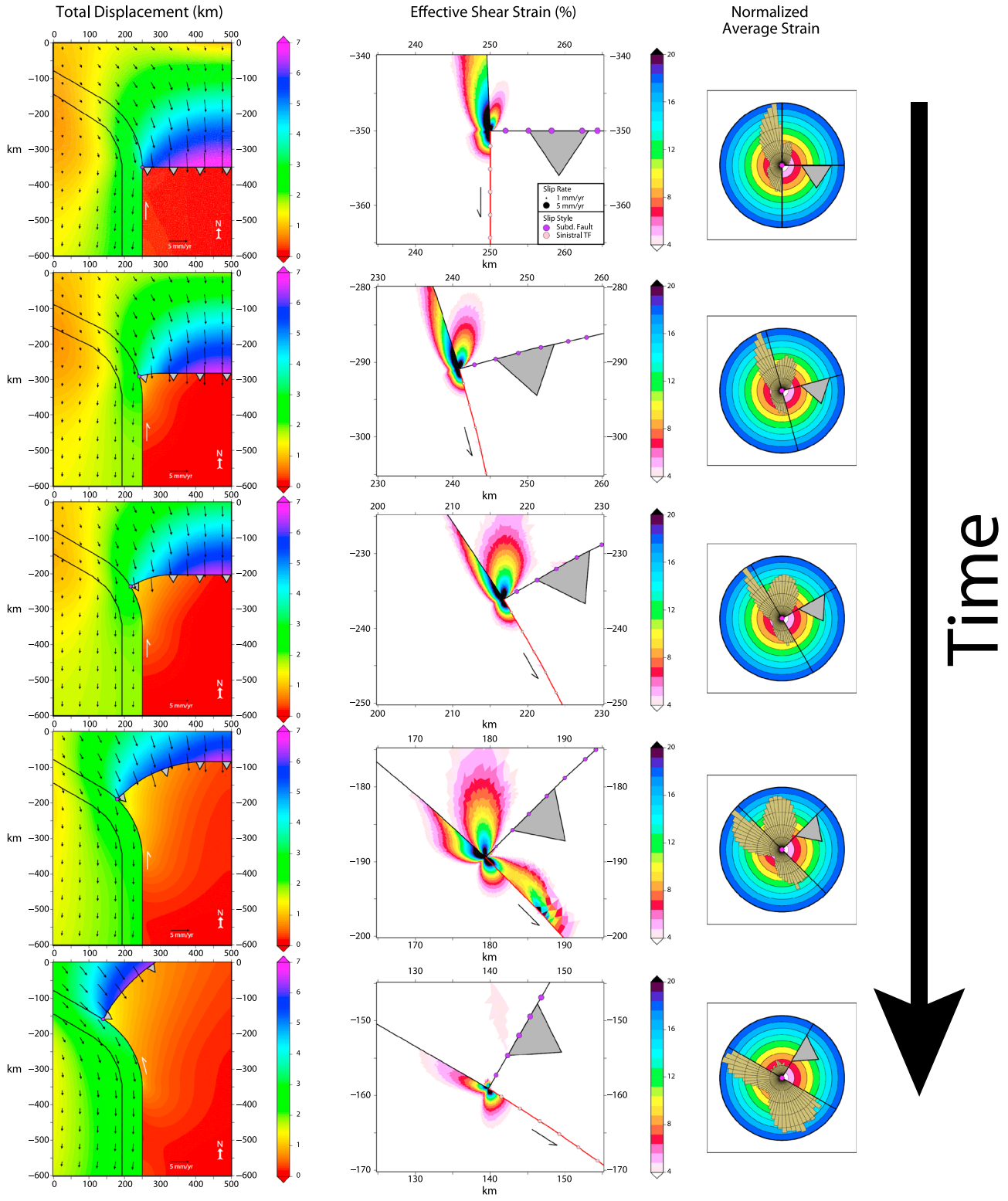

Figure 10. Model evolution series where β_k equals −60° and a radius of curvature of ~220 km. The contour plots show the (left column) total displacement and (middle column) effective shear strain. (right column) Pie charts of the normalized average strain within the first 10 km surrounding STEPs. Effective shear strain plots show the area directly around the STEP, while total displacement plots show the results for the whole models. In the displacement plots, velocity vectors are included for the continental-subducting plate block. The grey dents indicate the subduction direction, and the white slip symbol indicates the sinistral nature of the STEP fault. Slip rate magnitudes are the same as in Figure 4. The magenta hexagons represent the STEP. Every pie chart is normalized over the largest value of the average (effective shear) strain contained by a pie wedge. Color scale emphasizes this normalization. The black lines represent the passive margin orientation. For all models, *b* equals 0.02.

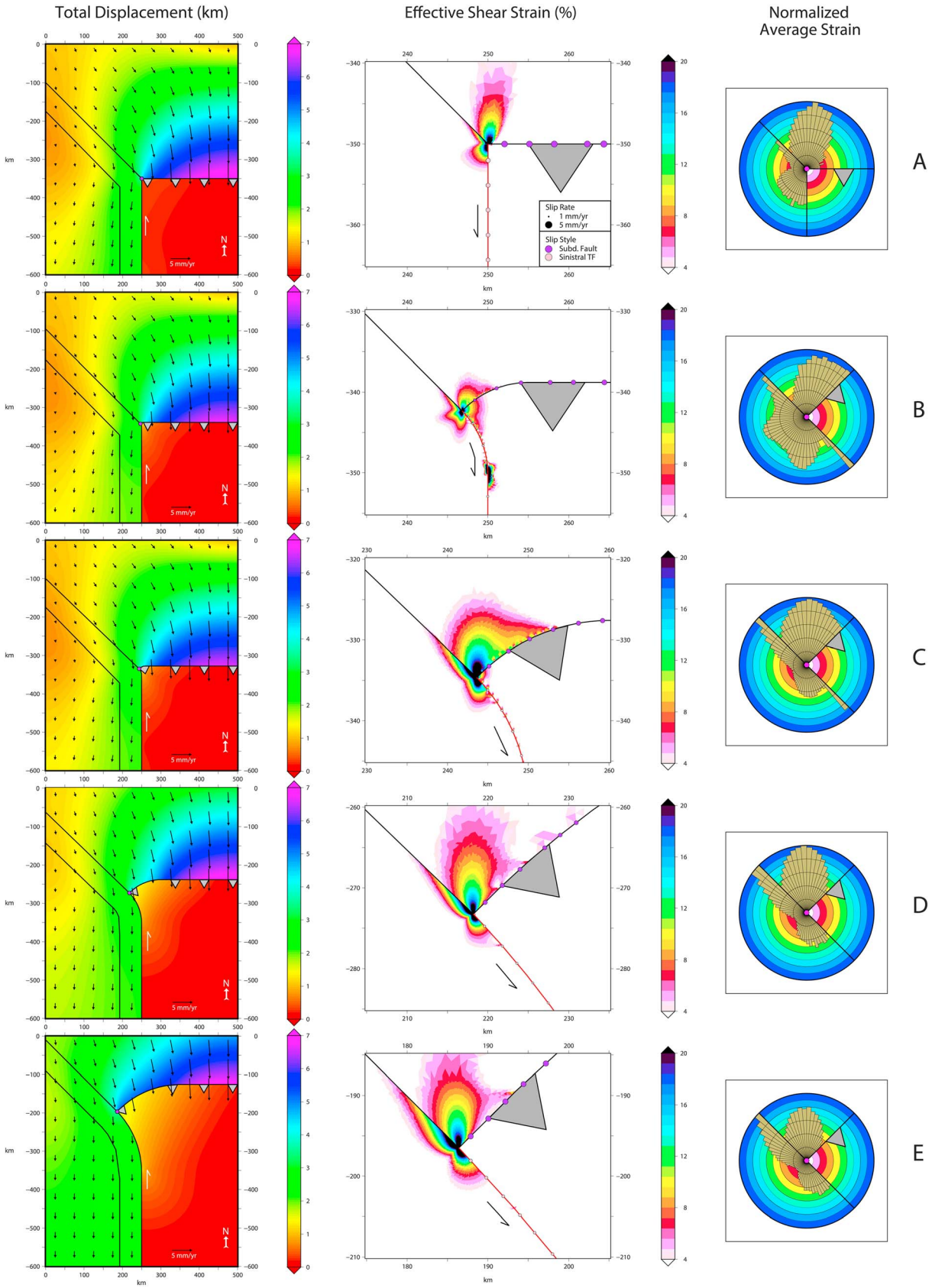
Total Displacement (km)
Effective Shear Strain (%)
Normalized Average Strain
Slip Rate
1 mm/yr
5 mm/yr
Slip Style
Subd. Fault
Sinistral TF
5 mm/yr
km
A
B
C
D
E

Figure 11

behavior of the STEP and a severe reduction in slip along the STEP fault toward the STEP (near zero). This is also represented in the normalized average strain plot, with a larger lobe of strain into the oceanic basin. The trench has lengthened (and curved) further, thereby increasing the formation of an amphitheatre-shaped slab.

At the last time step, the STEP has reached the end of the curve and the passive margin ahead of the STEP is finally oriented in the ideal direction as can be determined through the magnitudes of the slip along the STEP fault and across the trench which are larger than for the two previous model setups. STEP propagation will be along the passive margin. The trench-passive margin system now nearly represents a model where $\beta = 0$ (as in Figure 5) due to the extent of the passive margin-perpendicular segment of the trench.

6.5. STEP Model Results With Different Radii of Curvature for a β_k of 45°

From the previous section, it is clear that a large radius of curvature (~220 km) results in a STEP propagating along the passive margin, while a curved trench arises. This is in contrast to the behavior observed for an abrupt kink, where we see the STEP propagate into the oceanic basin (Figure 9 and Figure 11a). Now we seek to determine the minimum radius of curvature for which a STEP will propagate along the passive margin. In Figure 11, we present a series of model results for a range of radii of curvature. The nonabrupt models (Figures 11b–11e) represent setups where the STEP has propagated along the passive margin up to the point where the passive margin is oriented straight again and perpendicular to the trench.

For an abrupt kink, model results are depicted in Figure 11a. As was determined in the abrupt kink section, the STEP will propagate into the oceanic basin as the kink angle β_k of 45° is larger than 30°. When we introduce (and carefully increase) a radius of curvature to the STEP system, so that the change in orientation of the passive margin is distributed over a large distance, we observe different behavior (Figures 11b–11e). The amount of slip across trench and along the STEP fault has decreased compared to the abrupt kink setup (Figure 11a). Even though the STEP has propagated along the passive margin up to the point displayed at Figures 11b and 11c, the large buildup of effective shear strain in the subducting plate near the STEP is an indication that these setups are not favored by the system. The STEP will rather propagate into the oceanic basin when passing the 30–45° segment of the passive margin. We can thus conclude that the abrupt behavior is favored in case the radius of curvature is distributed through a radius of curvature of ~20 km. This means that one can consider the trench to remain straight over this distance and that the STEP system behaves as if the passive margin changes orientation in an abrupt kink.

In case the radius of curvature is distributed through a radius of curvature of ~125 km (Figure 11d), it is more difficult to determine STEP propagation direction. As was the case for the STEP system evolution in Figure 10, the segment of the trench perpendicular to the passive margin has lengthened. The amount of effective shear strain in the subducting plate along the trench has diminished, and we observe a single lobe. However, as can be determined from the normalized average strain plot, the peak strain is equally present in the passive margin. This model setup is settled at the end of a transition zone, where model setups show different behavior, from STEP propagation into the oceanic basin (as for Figures 11a–11c) toward clear STEP propagation along the passive margin (as in Figure 11e). There, the radius of curvature is equal to the model evolution series of Figure 10 and the observed propagation direction is the same: along the passive margin.

6.6. Analysis of Models With a Gradual Change in Passive Margin Orientation

Here we investigate the effect of a radius of curvature for the change in passive margin strike through a series of stylized model setups, based on the results from a previous time step. In case we test the influence of the magnitude of the velocity boundary condition at the northern domain boundary, we observe a difference in

Figure 11. Model series where β_k equals −45° with different radii of curvature: (a) 0 km, (b) ~10 km, (c) ~20 km, (d) ~125 km, and (e)~220 km. The contour plots show the (left column) total displacement and (middle column) effective shear strain. (right column) Pie charts of the normalized average strain within the first 10 km surrounding STEPs. Effective shear strain plots show the area directly around the STEP, while total displacement plots show the results for the whole models. In the displacement plots, velocity vectors are included for the continental-subducting plate block. The grey dents indicate the subduction direction, and the white slip symbol indicates the sinistral nature of the STEP fault. Slip rate magnitudes are the same as in Figure 4. The magenta hexagons represent the STEP. Every pie chart is normalized over the largest value of the average (effective shear) strain contained by a pie wedge. Color scale emphasizes this normalization. The black lines represent the passive margin orientation. For all models, *b* equals 0.02.

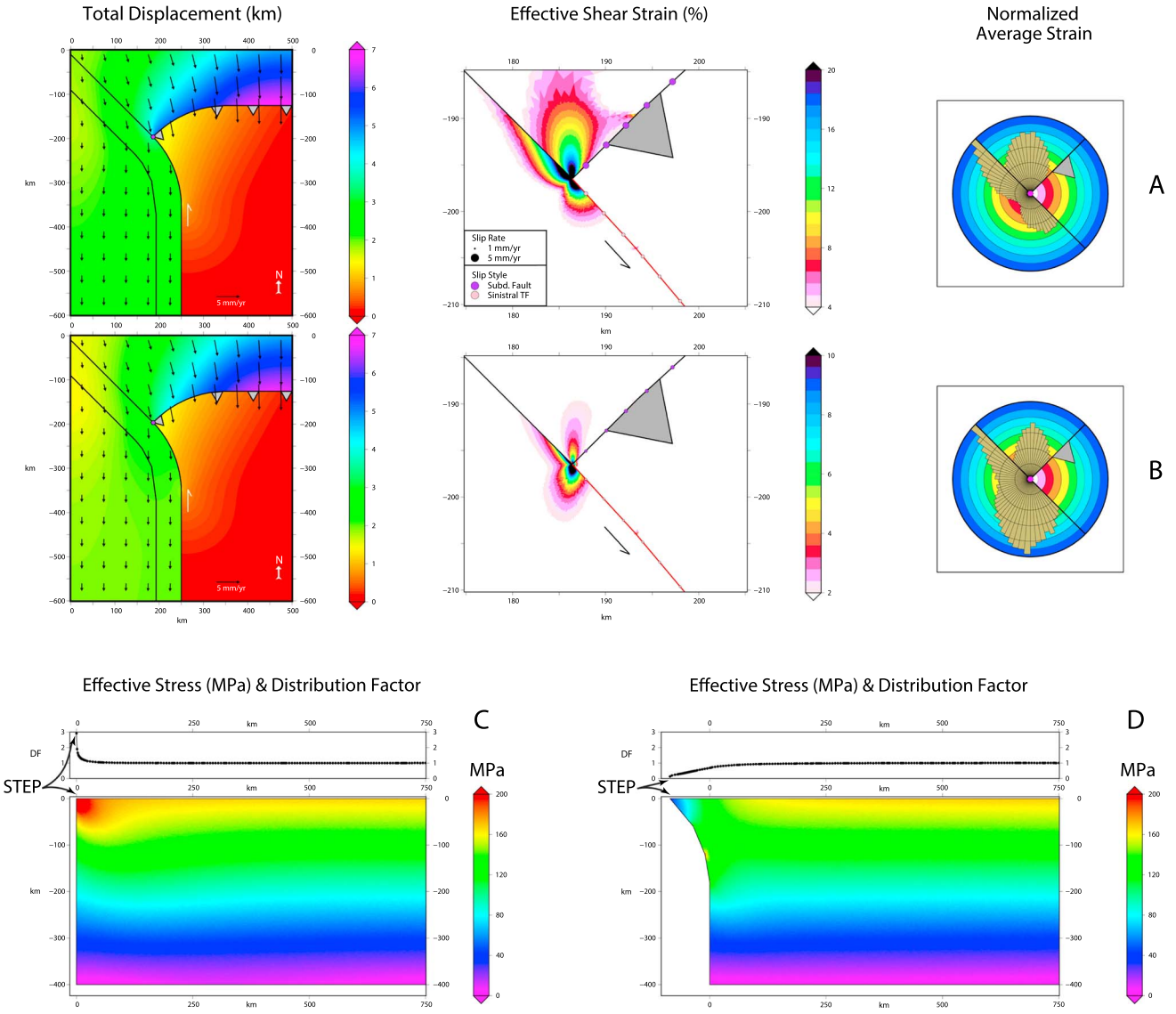

Figure 12. Comparison between (a and b) two models with (c and d) different forcing (respectively). The contour plots of Figures 12a and 12b show the (left column) total displacement and (middle column) effective shear strain. (right column) Pie charts of the normalized average strain within the first 10 km surrounding STEPs. Effective shear strain plots show the area directly around the STEP, while total displacement plots show the results for the whole models. In the displacement plots, velocity vectors are included for the continental-subducting plate block. The grey dents indicate the subduction direction, and the white slip symbol indicates the sinistral nature of the STEP fault. Slip rate magnitudes are the same as in Figure 4. The magenta hexagons represent the STEP. Every pie chart is normalized over the largest value of the average (effective shear) strain contained by a pie wedge. Color scale emphasizes this normalization. The black lines represent the passive margin orientation. Contour plots of Figures 12c and 12d show the effective stress experienced by the model slabs and the pattern of the distribution factor (explained in Appendix A) used for forcing of the STEP models in Figures 12a and 12b. For both models, *b* equals 0.02.

the magnitude of the slip, but not in the distribution pattern: slip is smallest near the STEP and increases away along trench. The rollback pattern does not change, only the velocity at which rollback takes place. Just as for the models with straight passive margins and abrupt kinks, the STEP will thus propagate in the same direction when altering the prescribed plate velocities.

One can consider that the shape of the slab after a considerable rollback, like at the two last model times in Figure 10 or Figure 11e, may be altered and that the slab pull transmission into the surface plate has consequently changed. However, in case we compare two end-member slab shapes, straight and shaped according to the passive margin (Figures 12c and 12d), we do not observe a change in the propagation behavior of the STEP (Figures 12a and 12b). The forcing is distinctly different in the region near the STEP, but the buildup of strain remains alongside the passive margin-ocean interface (Figure 12b). We can thus conclude that the

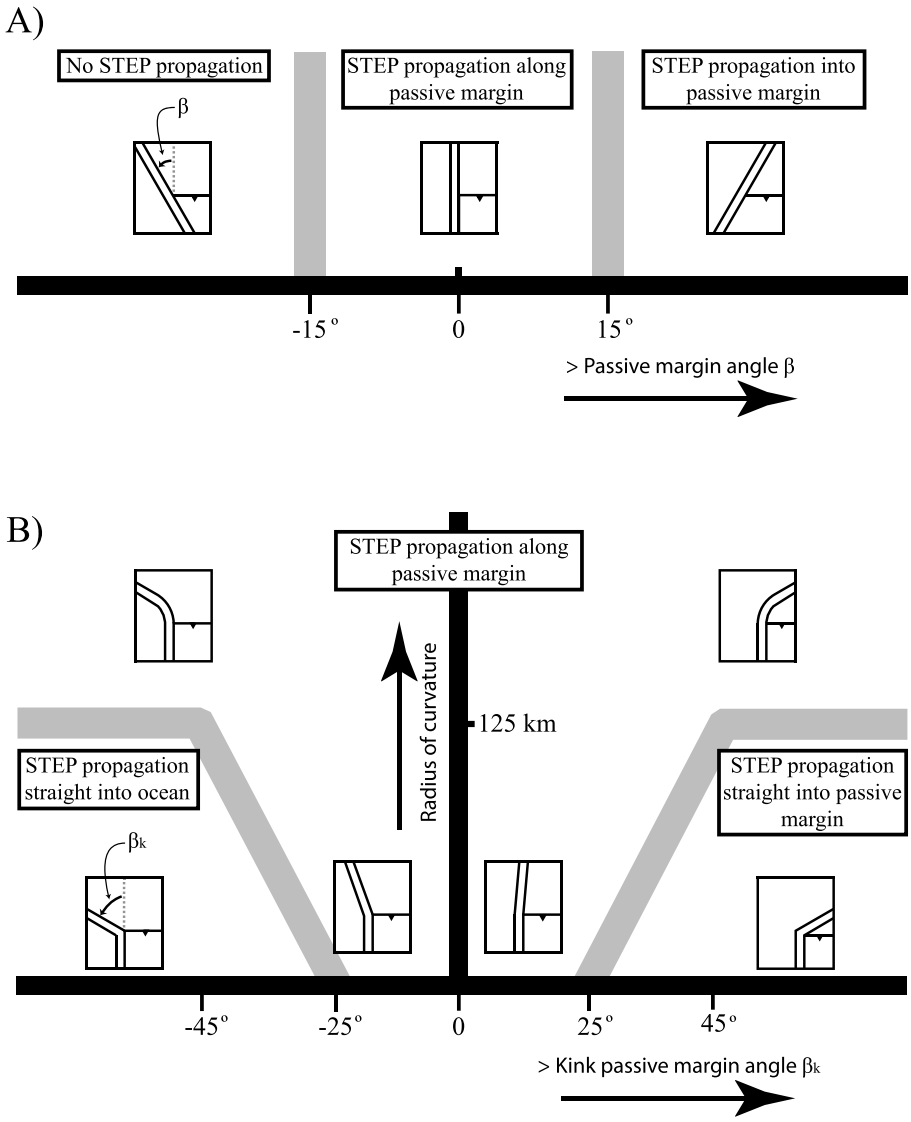

Figure 13. Schematic synthesis of model results indicating the STEP propagation (direction) behavior for passive margin geometry in case of (a) straight passive margins and (b) kinked passive margins. The grey bars indicate the transition between regimes where the STEP propagation direction is difficult to determine.

distribution of forcing at the trench also does not influence the STEP propagation direction, even though the rollback itself is slightly influenced from the presented model onward, as the amount of slip in the non-straight slab model (Figure 12b) is lower in magnitude than the slip in Figure 12a using a straight slab forcing.

7. Discussion

7.1. Summary of Model Response

In Figure 13 we summarize the STEP propagation behavior constrained from our model results for different passive margin geometries in a STEP setting. Here Figure 13a shows the straight passive margins while Figure 13b indicates the STEP propagation behavior for kinked passive margins. STEP propagation along straight passive margins occurs readily when oriented within 30° from a perpendicular setting. Our models show that a STEP system has the tendency to evolve toward a perpendicular geometry: for more negative passive margin angles, STEP propagation halts while the trench is able to rollback further toward orthogonality, while for more positive angles, the STEP will propagate more rapidly allowing the trench to "catch up" and return to orthogonality, while possibly, some continental material is pulled into the subduction zone which may result

in some local slab detachment. For some (narrow) subduction zones, e.g., the Gibraltar and Calabrian slabs, such rotation and reorientation toward orthogonality in order for the STEP to propagate along the passive margin have been suggested to explain the tectonic evolution in the western-central Mediterranean [*Govers and Wortel*, 2005; *Wortel et al*., 2009; *Chertova et al*., 2014a].

For STEP systems with a passive margin strike change less than 25° from perpendicular (ahead of the active STEP), STEPs will readily track the passive margin, irrespective of the radius of curvature through which this strike change is made (Figure 13b). Outside this window, i.e., for variable radii of curvature and larger (kink) passive margin angles, we observe two different types of propagation behavior. We find a "characteristic" radius of curvature of ~125 km, i.e., approximately the lithospheric thickness, where behavior changes: if the strike change is more gradual (larger than the lithospheric thickness), a STEP will continue to propagate along the passive margin, highlighting the steering effect of a passive margin. In case of an abrupt strike change (less than the lithospheric thickness), the STEP will continue to propagate in its original direction.

7.2. Limitations of the Numerical Models

The model results presented here provide straightforward indications for the propagation direction of STEPs and the influence of the mechanical properties. However, we employ several simplifications in our model setup. This includes a distinct determination of slab pull transmission at the trench, a stylized version of STEP geometry, a viscosity contrast across the passive margin, and ignoring upper mantle contributions to lithospheric behavior. Besides these simplifications in our models, we must consider whether our models actually represent a geodynamic system with a lithospheric tear (STEP and STEP fault) next to a subduction zone, comparable to those found in nature.

7.2.1. Effective Slab Pull Force

For the transmission of slab pull to the surface plate through the bending area at the trench, several resistive contributions, like mantle drag and friction along the plate contact zone, were accumulated in one reducing factor (Appendix A). In the STEP models studied here, the reducing factor was set at 0.5 for all models. We consider that, as the radiation pattern also does not change for decreasing slab pull magnitudes or a change in the viscosity contrast across the trench (Appendix B), altering the reducing factor does not result in different STEP propagation directions (Figure S4).

7.2.2. Geometric Complexity Near STEPs and STEP Faults

STEP geometries used in these numerical STEP models are stylized versions of situations as found in nature. Often, the trench does not run perfectly perpendicular to the passive margin, and the trench shows a nonlinear profile. From the model results, it is clear that small changes ($<10°$) in the trench-passive margin setup do not result in large changes in STEP behavior. Therefore, the STEP models appear to be relatively insensitive to small-scale details. As such, we can consider that a propagating STEP will simply follow a straight path in case a passive margin displays a rugged shape in map view, i.e., with (relatively) small but abrupt and oblique bulges. A propagating STEP will simply skip such heterogenic features.

7.2.3. Mantle Flow

In the models studied here, mantle contributions to the lithospheric behavior were ignored. Several studies on mantle return flow and toroidal mantle flow have been performed recently by *Piromallo et al*. [2006], *Schellart et al*. [2007], *Hale et al*. [2010], *Schellart* [2010], and *Schellart and Moresi* [2013], among others. Mantle flow has an influence on the state of stress and vertical motion of both the overriding and subducting plates, subduction hinge geometry, and associated volcanism [*Faccenna et al*., 2011; *Schellart and Moresi*, 2013]. *Schellart et al*. [2007] show through 3-D, dynamic, numerical models that rollback velocity (trench retreat rate) and trench width are inversely related for free subduction experiments, consistent with globally observed retreat velocities. Mantle material seems to influence the geometry of the trench, especially near the lateral termination of a subduction zone, explicitly related to the width of the trench. A trench retreats, and a concave geometry toward the mantle wedge edge arises. This is in agreement with several situations found in nature, e.g., the south Lesser Antilles subduction zone. Rollback velocity is very likely to be largely influenced by mantle flow [e.g., *Schellart et al*., 2007; *Schellart and Moresi*, 2013], e.g., by a mantle wind, trench suction due to poloidal flow, and/or mantle return flow around the slab edge. This is probably not the case for the propagation direction of the STEP (slab tear), where a surface part of the plate and an overriding plate are part of the system. Material properties and the orientation of a viscosity contrast have a large influence on the STEP propagation direction [*Hale et al*., 2010].

7.2.4. Variations With Depth in the Lithosphere

As we set our model lithosphere as a single layer with a single viscosity, we ignore the layer-by-layer distribution of material properties and (possible) intricate pattern of faults present in Earth's lithosphere. We consider that, with the implementation of a viscosity contrast across the passive margin and the development of a shear zone in our models, the lithosphere tearing character of STEP faults is underpinned (despite the simplified mechanism of strain localization).

7.2.5. Magmatic Arcs and Other Additional Zones of Weakness

In our STEP models, we do not include the possible effect of a weak magmatic arc [*Boutelier and Cruden*, 2013] as we simply take one value for the effective viscosity per whole subdomain. This may have an effect on the motion of the overriding plate, i.e., increasing the ease to follow the retreating trench [*Govers and Wortel*, 2005]. Especially through the models with a radius of curvature where we need to go through an evolution series, the eventual trench location resulting from rollback may change significantly when introducing the effect of a weak magmatic arc. However, as we have already observed in all models, the STEP propagation direction does not actually depend on the exact distribution of material properties (Appendix B) but rather on a contrast in properties directly ahead of the STEP. This does not only encompass passive margins but also other weakness zones, like fracture and fault zones, and strong regions, like oceanic plateaus or seamount chains.

7.2.6. Brittle Rheology

The omission of brittle behavior may potentially have a large effect on the direction of STEP propagation. This is especially the case in situations where a large differential stress develops ahead of the STEP. *Hale et al*. [2010] consider 3-D, dynamic numerical models that include visco-plastic weak zones at the sides of the subduction zone (at a 90° angle from the trench) in order to obtain a first-order view on lithospheric tear dynamics in subduction zone settings. These authors find that lithospheric resistance to tearing is essential in the evolution of a rollback system with regard to hinge geometry, rollback velocity, and slab behavior in the mantle. In case the yield strength of the weak layer has values in the 25–100 MPa range, the subduction hinge will show a curvature toward the mantle wedge side and slab rollback velocity increases away from the slab STEP. According to *Hale et al*. [2010], the yield strength of the weak layer controls the geometry of the subduction system and mantle flow becomes less important while increasing the yield strength.

Our model results, with a viscosity contrast and $\beta = 0°$, are comparable to the models of *Hale et al*. [2010] in setup. Models with an intermediate yield strength for the weak layer (25–100 MPa) show similar behavior as our model results, where a curved (toward the mantle wedge side) geometry of the subduction contact arises and a transform motion arises at the edge of the weak layer. Even though the models of *Hale et al*. [2010] ignore elastic behavior and therefore neglect the notion of slab pull transmission into the surface plate, there is an overall consensus with our results on tear propagation and trench geometry.

From STEP models for the westernmost Mediterranean, *Chertova et al*. [2014a, 2014b] conclude that the North African continental margin needs to be "weak" with a maximum shear strength of 100 MPa for STEP propagation to take place. Besides this indication of a weak (African) continental margin along which a STEP retreated, the resulting (present) curvature of the Gibraltar trench [*Gutscher et al*., 2012] is also in agreement with our findings and the results of *Hale et al*. [2010]. We therefore suspect that our omission of brittle behavior does not significantly affect our conclusions, but this remains a topic of further (3-D) studies.

7.2.7. Surface Velocities

We find that far-field velocities do not significantly affect the STEP propagation direction. This result contrasts with those of *Chertova et al*. [2014b]. When the velocity perpendicular to the STEP fault is large enough, we do expect inversion of the STEP fault in a manner as described by *Baes et al*. [2011].

7.3. Comparison With STEP Settings in Nature

7.3.1. Northern Tonga

Our uniform model results (Figure 4) should be applicable to the northern end of the Tonga subduction zone, where the trench is retreating with a very high velocity. The Tonga trench shows a geometry that is concave to the mantle wedge side and (sub) perpendicular to the (trace of the) STEP fault (i.e., the Vityaz lineament [*Wortel et al*., 2009; *Schellart and Spakman*, 2012]). This lines up with our uniform model results, which predict

a propagation direction of ~80° ahead of the active STEP. Even though our model is not designed to represent the geodynamic setting at the Tonga trench in every detail, such as plate and rollback velocities, it still predicts this propagation direction well. We can therefore infer that mantle (return) flow does not significantly affect the direction of lithospheric tearing.

Unlike *Clouard and Gerbault* [2008], who relate intraplate volcanism in the south-central Pacific to the geometry and kinematics of the Pacific plate, we expect the effect of lithospheric tearing at the northern termination of the Tonga trench to be constrained to the immediate vicinity of the STEP. There is no indication from our models that the effect of the edge of the subducting plate will radiate far into the surface part of the subducting plate. This leads us to conclude that the inference by *Clouard and Gerbault* [2008] is a result of boundary conditions applied in their models, while this inference cannot be construed in view of a tearing Pacific plate at the northern termination of the Tonga trench, as suggested by our models.

7.3.2. Southern Lesser Antilles

Related to the STEP at the southern termination of the south Lesser Antilles trench, model results confirm the stable setup of a STEP propagating along a straight passive margin which is oriented perpendicular to the trench. The slab shows a concave geometry toward the mantle wedge side (Figure 2 [*Clark et al*., 2008]), probably resulting from resistance to lithospheric tearing. This concave (to the mantle wedge side) geometry is also a feature observed in our numerical models. We observe for models with a very positive β that the passive margin is pulled into the subduction zone (Figures 5, 8, and 13). This will probably result in a higher resistance to subduction locally, a slowdown in subduction, and possibly local slab detachment (the shoaling mechanism in *Wortel et al*. [2009]) which de facto enables the STEP to keep following the passive margin. Geological reconstructions of the Lesser Antilles trench indicate that this mechanism has probably prevailed for the Caribbean-South American boundary [e.g., *Escalona and Mann*, 2011; *van Benthem et al*., 2013]. We must note here that the development of a STEP and STEP fault in our models is simplified as we consider a single fault for the STEP fault and a localized shear zone for the STEP propagation, while in reality this may involve a broad, complex zone of deformation including block rotations in a wider shear zone observed in the geological plate boundary zone [*Govers and Wortel*, 2005; *Martin*, 2007; *Wortel et al*., 2009; *Özbakir et al*., 2013]. Now that the STEP has reached the eastern edge of the South American continental margin, the passive margin is rotating away from the trench at such an oblique angle that we suspect the STEP to propagate into the Atlantic rather than keep following the South American continental domain in the geological future. This is based on the notion of the models with kinks in passive margin orientation which show that, if the gap is too large to bridge, the STEP will propagate into the oceanic basin.

8. Conclusions

Numerical models presented here indicate that a STEP will propagate along a straight passive margin in case the angle between trench and passive margin remains within 15° from a perpendicular setup. The response to a change in strike of a passive margin depends on how abrupt this occurs. For an abrupt change, i.e., when the radius of curvature is smaller than the lithosphere thickness, the STEP will continue to track the passive margin if the strike change is less than 25°. If the change in passive margin orientation is larger, the STEP will continue to propagate in the original direction. For a gradual change, i.e., when the radius of curvature is larger than the lithosphere thickness, the STEP will continue to propagate along the passive margin.

The mechanical evolution of STEP systems results in a geometry where trench and STEP fault are perpendicular, in correspondence with the observed STEPs in nature. If the geometry for some reason is strongly oblique, the system evolves to become more orthogonal due to reorientation of the trench.

Numerical model results are relatively insensitive to smaller-scale details, such as small ($<$10°) variations in passive margin orientation. This also indicates that a slab tear will simply propagate as a straight feature in case a passive margin has rugged shape in map view. The influence of crustal-scale heterogeneities is thus quasi-inexistent compared with the large stresses producing the tearing of the lithosphere by slab pull.

Surprisingly, the magnitudes of the strength contrast across the passive margin and the subduction history, which determines the resistance to lithospheric tearing and the forcing at the trench, respectively, are less important. These only affect intensity of deformation but not the propagation direction of a STEP.

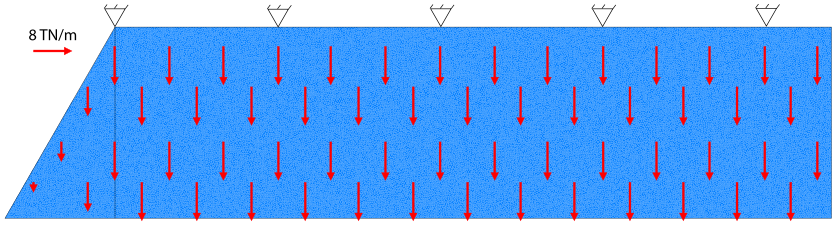

Figure A1. Schematic 2-D view of the slab as seen from a dip-perpendicular view. The topside is kept at its place. The red arrows indicate the slab pull. The model shown here corresponds to a situation where the passive margin has a positive angle β of 30°.

Appendix A: Slab Pull-Associated Tractions

Since the velocity of a slab is approximately constant during the descent into the mantle, the slab must be in mechanical equilibrium. Therefore, the sum of all external forces acting upon the slab is zero. Both resistive and driving forces act on a subducting and surface plate [*McKenzie*, 1969]. The forces acting on the subducting plate, per unit length at interfaces or area, and their magnitudes can consequently be determined by an integration over the appropriate area [*Wortel et al*., 1991]. Slab pull is the only force which can be described to a reasonable extent though [*Schellart*, 2004b].

An important assumption made in the following is that all parameters of the subducting lithospheric plate (including the surface part) are constant. This includes the thickness, temperature distribution, and density, among others. Another assumption made is that mantle flow is not actively causing plate motion but does result from the plate motions. Therefore, we regard mantle flow as a passive consequence caused by resistive forces acting on sides of the slab.

In order to determine the pattern of transmitted slab pull forces, we model a subducting slab with a slab pull acting on it, while keeping the topside in place. All other boundaries besides the topside are free, i.e., not obligated to follow the direction of the slab pull (see Figure A1). The mechanical equilibrium equations are consequently solved using the GTECTON software (version 2011.1.65) adopting the plane stress approximation.

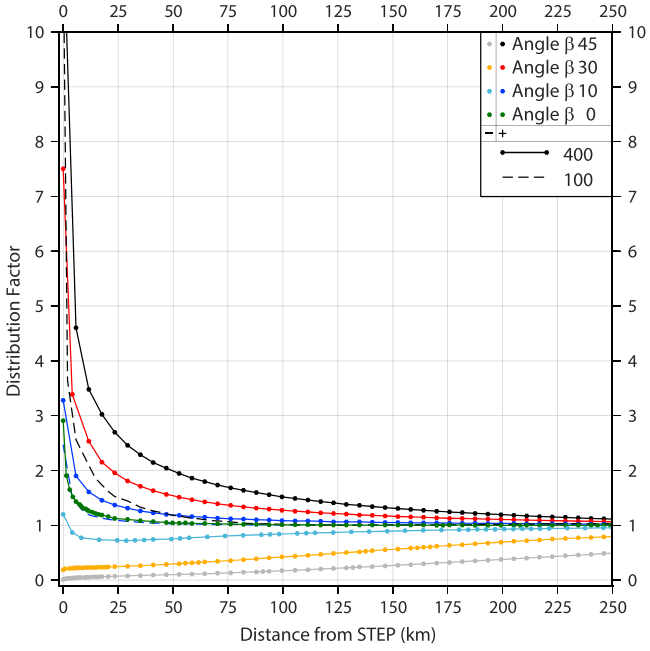

Figure A2. The distribution factor as a function of distance along the trench (distance from STEP). Colors indicate the angle of the passive margin β. For these models, slab length is 400 km as represented by the solid lines with dots. The dashed lines indicate the two models with a slab length of 100 km.

Slab pull is modeled as a shear traction acting on the top of the slab, acting downdip. We use an elastic plate with a thickness of 1 m. Elastic parameters are taken constantly for the whole slab: Young's modulus E is 75 GPa and Poisson's ratio v is 0.25. Slab geometry is a major control on the distribution of the forces. Horizontal distance of the slab model is 1500 km for all models, to ensure that the lateral sides do not affect the opposite side of the slab and avoid the use of lateral boundary conditions. The slab is free to move in all directions as a result from the slab pull.

Resulting values for the forces required to keep the topside of the plate at its place are normalized by a value taken far away from the lateral slab boundaries. At such locations, a "nonaffected equilibrium" exists, not affected by variations in slab geometry or gradients

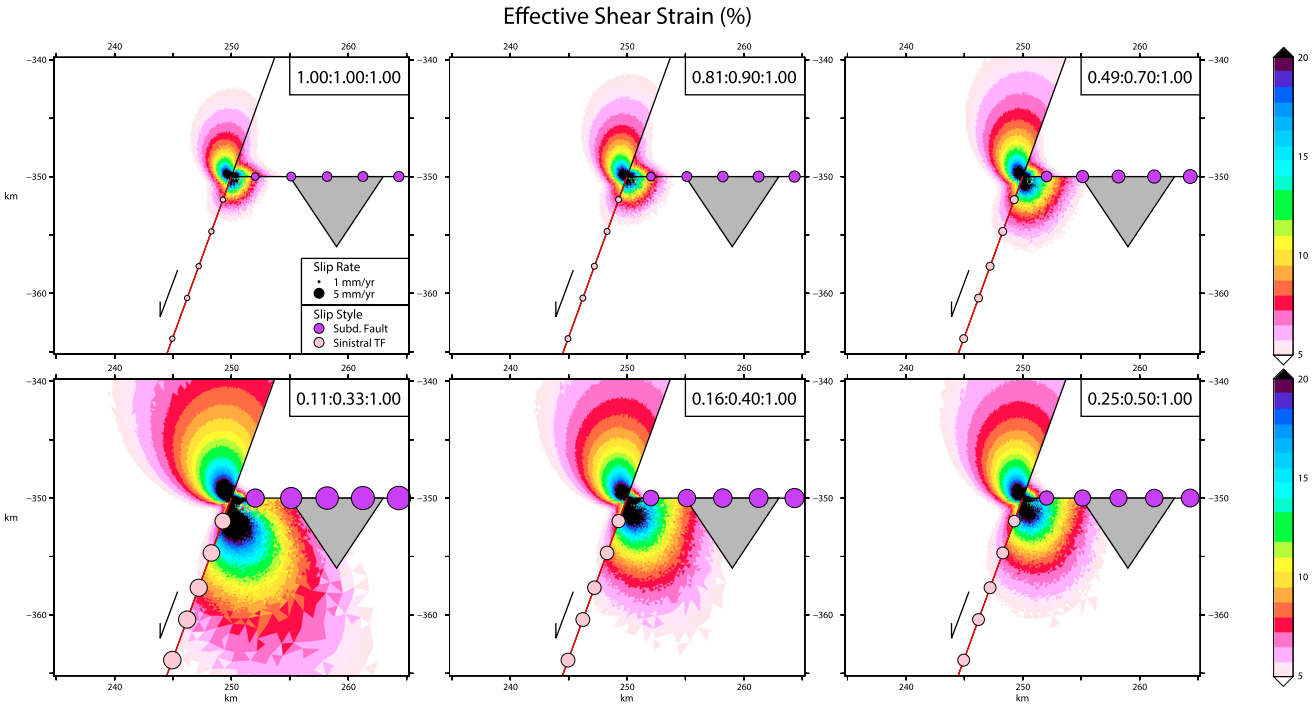

Figure B1. Model results of the effective shear strain for a range of viscosity contrasts across the passive margin (boxes) and a β of 25°. These plots show the area directly around the STEPs. The grey dent indicates the subduction direction. Slip rate magnitudes are the same as in Figure 4. For viscosity contrasts 1:1, 0.9:1, 0.7:1, 0.5:1, 0.4:1, and 0.33:1, *b* equals 9.5, 0.5, 0.5, 0.5, 0.5, and 9.5, respectively.

in the slab pull. We define these values as a distribution factor (DF). At the top edge where an equilibrium exists with no influence of slab geometry and slab pull gradients, the DF will have a value of 1. Deviations from a value of 1 then represent effects due to lateral slab boundaries and/or gradients in slab pull.

Passive margin angle β in the positive quadrant results in DF values of well over 1 near the STEP with a 1/r distribution decreasing away from the STEP. Passive margin angles in the negative quadrant result in DF values which slowly increase from 0 and have a larger slab edge influence distance than the same passive margin angle β in the positive quadrant. For models where β is close to 0°, the DF pattern shows a value above 1, even when the angle lies in the negative quadrant. This is mainly due to elasticity of the plate, but gradient in slab pull also controls the transmission pattern.

For every possible STEP setup, a specific numerical slab model needs to be monitored in order to accurately describe the transmission pattern of the slab pull. Resistive forces are captured in a reducing factor which is set at 0.5. This factor depends on multiple characteristics of the STEP system: plate viscosity, slab density, and the mantle-plate viscosity contrast among others. The value of 0.5 is based on two notions: (1) a comparison of plate bending and its consequences on slab pull transmission [*Capitanio et al.*, 2009] and (2) a study on the influence of slab pull and laterally variable asthenosphere in a global plate motion model [*van Summeren et al.*, 2012].

Appendix B: The Viscosity Contrast Across the Passive Margin

In the numerical STEP models presented in this report, we employ a viscosity contrast across the passive margin in order to represent a change in lithospheric strength from ocean to continent. We applied a contrast of 0.25:0.50:1 in the presented model results, where the ocean lithospheric viscosity is set at 1. However, we need to determine the influence of the magnitude of this contrast and ascertain whether the propagation direction of a STEP is altered in case we choose a different viscosity contrast in our models.

In Figure B1 we depict several models with different contrasts in viscosity across the passive margin. It is clear that a lower effective viscosity results in a larger effective shear strain buildup, while the extent of the

deformation lobe is reduced for larger magnitudes of the effective viscosity. This is a very logical observation as the strain depends directly on viscosity. The overall deformation pattern remains the same in case we change the magnitude of the viscosity contrast across the passive margin, and we can conclude that this does not affect the propagation direction of a STEP (fault).

Acknowledgments

All figures, except Figures 1, 2, and 7a, were generated using the GMT software by *Wessel and Smith* [1991]. Input and output files and the software source codes that were used for the models of this paper are digitally stored at Utrecht University. Digital copies of the output files can be made available upon request to the corresponding author. We would like to thank Vincent Strak, Wouter Schellart, Paul Tregoning, and an anonymous reviewer for their accurate and constructive comments, which helped to improve the original manuscript. N.N. is funded by project EURAF 2.1.11 of ISES, Netherlands Research Centre for Integrated Solid Earth Science.

References

Austermann, J., J. X. Mitrovica, K. Latchyev, and G. A. Milne (2013), Barbados-based estimate of ice volume at Last Glacial Maximum affected by subducted plate, *Nat. Geosci.*, *6*, doi:10.1038/NGEO1859.

Baes, M., R. Govers, and R. Wortel (2011), Subduction initiation along the inherited weakness zone at the edge of a slab: Insights from numerical models, *Geophys. J. Int.*, *184*, 991–1008.

Bijwaard, H., and W. Spakman (2000), Nonlinear global *P*-wave tomography by iterated linearized inversion, *Geophys. J. Int.*, *141*, 71–82.

Bos, B., and C. Spiers (2002), Frictional-viscous flow of phyllosilicate-bearing fault rock: Microphysical model and implications for crustal strength profiles, *J. Geophys. Res.*, *107*(B2), 2028, doi:10.1029/2001JB000301.

Boutelier, D., and A. Cruden (2013), Slab rollback rate and trench curvature controlled by arc deformation, *Geology*, *41*(8), 911–914, doi:10.1130/G34338.1.

Burov, E. (2011), Rheology and strength of the lithosphere, *Mar. Pet. Geol.*, *28*, 1402–1443.

Calignano, E., D. Sokoutis, E. Willingshofer, F. Gueydan, and S. Cloetingh (2015), Strain localization at the margins of strong lithospheric domains: Insights from analog models, *Tectonics*, *34*, 396–412, doi:10.1002/2014TC003756.

Capitanio, F. A., G. Morra, and S. Goes (2009), Dynamic of plate bending at the trench and slab-plate coupling, *Geochem. Geophys. Geosyst.*, *10*, Q04002, doi:10.1029/2008GC002348.

Chertova, M. V., W. Spakman, T. Geenen, A. P. van den Berg, and D. J. J. van Hinsbergen (2014a), Underpinning tectonic reconstructions of the western Mediterranean region with dynamic slab evolution from 3-D numerical modelling, *J. Geophys. Res. Solid Earth*, *119*, 5876–5902, doi:10.1002/2014JB011150.

Chertova, M. V., W. Spakman, A. P. van den Berg, and D. J. J. van Hinsbergen (2014b), Absolute plate motions and regional subduction evolution, *Geochem. Geophys. Geosyst.*, *15*, 3780–3792, doi:10.1002/2014GC005494.

Clark, S. A., M. Sobiesiak, C. A. Zelt, M. B. Magnani, M. S. Miller, M. J. Bezada, and A. Levander (2008), Identification and tectonic implications of a tear in the South American plate at the southern end of the Lesser Antilles, *Geochem. Geophys. Geosyst.*, *9*, Q11004, doi:10.1029/2008GC002084.

Clouard, V., and M. Gerbault (2008), Break-up spots: Could the Pacific open as a consequence of plate kinematics?, *Earth Planet. Sci. Lett.*, *265*, 195–208.

Dayem, K. E., G. A. Houseman, and P. Molnar (2009), Localization of shear along a lithospheric strength discontinuity: Application of a continuous deformation model to the boundary between Tibet and the Tarim Basin, *Tectonics*, *28*, TC3002, doi:10.1029/2008TC002264.

De Franco, R., R. Govers, and R. Wortel (2008), Dynamics of continental collision: Influence of the plate contact, *Geophys. J. Int.*, doi:10.1111/j.1365-246X.2008.03857.x.

England, P., and G. Houseman (1985), Role of lithospheric strength heterogeneities in the tectonics of Tibet and neighbouring regions, *Nature*, *315*, 297–301.

England, P., and D. McKenzie (1982), A thin viscous sheet model for continental deformation, *Geophys. J. R. Astron. Soc.*, *70*, 295–321.

Escalona, A., and P. Mann (2011), Tectonics, basin subsidence, and paleogeography of the Caribbean-South American plate boundary zone, *Mar. Pet. Geol.*, *28*, 8–39.

Faccenna, C., P. Molin, B. Orecchio, V. Olivetti, O. Bellier, F. Funiciello, L. Minelli, C. Piromallo, and A. Billi (2011), Topography of the Calabria subduction zone (southern Italy): Clues for the origin of Mt. Etna, *Tectonics*, *30*, TC1003, doi:10.1029/2010TC002694.

Forsyth, D. W. (1975), Fault plane solutions and tectonics of the South Atlantic and Scotia Sea, *J. Geophys. Res.*, *80*(11), 1429–1443, doi:10.1029/JB080i011p01429.

Goetze, C., and B. Evans (1979), Stress and temperature in the bending lithosphere as constrained by experimental rock mechanics, *Geophys. J. R. Astron. Soc.*, *59*, 463–478.

Govers, R., and M. Wortel (1999), Some remarks on the relation between vertical motions of the lithosphere during extension and the necking depth parameter inferred from kinematic modelling studies, *J. Geophys. Res.*, *104*, 23, 245–23, 253, doi:10.1029/1999JB900201.

Govers, R., and M. J. R. Wortel (2005), Lithosphere tearing at STEP faults: Response to edges of subduction zones, *Earth Planet. Sci. Lett.*, *236*, 505–523.

Gudmundsson, O., and M. Sambridge (1998), A regionalized upper mantle (RUM) seismic model, *J. Geophys. Res.*, *103*(B4), 7121–7136, doi:10.1029/97JB02488.

Gutscher, M.-A., et al. (2012), The Gibraltar subduction: A decade of new geophysical data, *Tectonophysics*, *574–575*, 72–91.

Hale, A. J., K.-D. Gottschaldt, G. Rosenbaum, L. Bourgouin, M. Bauchy, and H. Mülhaus (2010), Dynamics of slab tear faults: Insights from numerical modelling, *Tectonophysics*, *483*, 58–70.

Hall, R. (2002), Cenozoic geological and plate tectonic evolution of SE Asia and the SW Pacific: Computer-based reconstructions, model and animations, *J. Asian Earth Sci.*, *20*, 353–431.

Hall, R., and W. Spakman (2002), Subducted slabs beneath the eastern Indonesia-Tonga region: Insights from tomography, *Earth Planet. Sci. Lett.*, *201*, 321–336.

Hayes, G. P., D. J. Wald, and R. L. Johnson (2012), Slab1.0: A three-dimensional model of global subduction zone geometries, *J. Geophys. Res.*, *117*, B01301, doi:10.1029/2011JB008524.

Isacks, B., L. Sykes, and J. Oliver (1969), Focal mechanisms of deep and shallow earthquakes in the Tonga-Kermadec region and the tectonics of island arcs, *Geol. Soc. Am. Bull.*, *18*, 1443–1470.

Kohlstedt, D. L., B. Evans, and S. J. Mackwell (1995), Strength of the lithosphere: Constraints imposed by laboratory experiments, *J. Geophys. Res.*, *100*(B9), 17,587–17,602, doi:10.1029/95JB01460.

Martin, A. K. (2007), Gondwana breakup via double-saloon-door rifting and seafloor spreading in a backarc basin during subduction rollback, *Tectonophysics*, *445*, 245–272.

McKenzie, D. P. (1969), Speculations on the consequences and causes of plate motions, *Geophys. J. R. Astron. Soc.*, *18*, 1–32.

Melosh, H. J., and C. A. Williams (1989), Mechanics of graben formation in crustal rocks: A finite element analysis, *J. Geophys. Res.*, *94*, 13,961–13,973, doi:10.1029/JB094iB10p13961.

Millen, D. W., and M. W. Hamburger (1998), Seismological evidence for tearing of the Pacific plate at the northern termination of the Tonga subduction zone, *Geology*, *26*, 659–662.
Özbakir, A. D., A. M. C. Şengör, M. J. R. Wortel, and R. Govers (2013), The Pliny-Strabo trench region: A large shear zone resulting from slab tearing, *Earth Planet. Sci. Lett.*, *325*, 188–195.
Piromallo, C., T. W. Becker, F. Funiciello, and C. Faccenna (2006), Three-dimensional instantaneous mantle flow induced by subduction, *Geophys. Res. Lett.*, *33*, L08304, doi:10.1029/2005GL025390.
Plattner, C., R. Malservisi, and R. Govers (2009), On the plate boundary forces that drive and resist Baja California motion, *Geology*, *37*, 359–362.
Ranalli, G. (1995), *Rheology of the Earth*, 2nd ed., Chapman and Hall, London, U. K.
Regenauer-Lieb, K., and D. Yuen (1998), Rapid conversion of elastic energy into plastic shear heating during incipient necking of the lithosphere, *Geophys. Res. Lett.*, *25*(14), 2737–2740, doi:10.1029/98GL02056.
Schellart, W. P. (2004a), Kinematics of subduction and subduction-induced flow in the upper mantle, *J. Geophys. Res.*, *109*, B07401, doi:10.1029/2004JB002970.
Schellart, W. P. (2004b), Quantifying the net slab pull force as a driving mechanism for plate tectonics, *Geophys. Res. Lett.*, *31*, L07611, doi:10.1029/2004GL019528.
Schellart, W. P. (2010), Mount Etna-Iblean volcanism caused by rollback-induced upper mantle upwelling around the Ionian slab edge: An alternative to the plume model, *Geology*, *38*, 691–694.
Schellart, W. P., and L. Moresi (2013), A new driving mechanism for backarc extension and backarc shortening through slab sinking induced toroidal and poloidal mantle flow: Results from dynamic subduction models with an overriding plate, *J. Geophys. Res. Solid Earth*, *118*, 3221–3248.
Schellart, W. P., and W. Spakman (2012), Mantle constraints on the plate tectonic evolution of the Tonga-Kermadec-Hikurangi subduction zone and the South Fiji Basin region, *Aust. J. Earth Sci.*, *59*, 933–953.
Schellart, W. P., J. Freeman, D. R. Stegman, L. Moresi, and D. May (2007), Evolution and diversity of subduction zones controlled by slab width, *Nature*, *446*, doi:10.1038/nature05615.
Sibson, R. H. (1977), Fault rocks and fault mechanisms, *J. Geol. Soc. London*, *133*, 191–213.
Steinberger, B., and A. R. Calderwood (2006), Models of large-scale viscous flow in the Earth's mantle with constraints from mineral physics and surface observations, *Geophys. J. Int.*, *167*, 1461–1481, doi:10.1111/j.1365-246X.2006.03131.x.
van Benthem, S., R. Govers, W. Spakman, and R. Wortel (2013), Tectonic evolution and mantle structure of the Caribbean, *J. Geophys. Res. Solid Earth*, *118*, 3019–3036.
van Summeren, J., C. P. Conrad, and C. Lithgow-Bertelloni (2012), The importance of slab pull and a global asthenosphere to plate motions, *Geochem. Geophys. Geosyst.*, *13*, Q0AK03, doi:10.1029/2011GC003873.
Wessel, P., and W. H. F. Smith (1991), Free software helps map and display data, *Eos Trans. AGU*, *72*, 441, doi:10.1029/90EO00319.
Wilson, J. T. (1965), A new class of faults and their bearing on continental drift, *Nature*, *207*, 343–347.
Wortel, M. J. R., M. J. N. Remkes, R. Govers, S. A. P. L. Cloetingh, and P. T. Meijer (1991), Dynamics of the lithosphere and the intraplate stress field, *Phil. Trans. R. Soc. A*, *337*, 111–126.
Wortel, R., R. Govers, and W. Spakman (2009), STEP-wise evolution of convergent plate boundaries: From structure to dynamics, in *Subduction Zone Geodynamics*, edited by S. Lallemand and F. Funiciello, Springer, Berlin, Heidelberg, doi:10.1007/978-3-540-87974-9.